

พลวัตเชิงโมเลกุลของโปรตีนเอ็ม-2 แชนแนลของไวรัสฮินฟลูเอ็นซาเอ



นางสาวจิตติมา เล่าห์พงศ์ไพศาล

สถาบันวิทยบริการ
จุฬาลงกรณ์มหาวิทยาลัย

วิทยานิพนธ์นี้เป็นส่วนหนึ่งของการศึกษาตามหลักสูตรปริญญาวิทยาศาสตรดุษฎีบัณฑิต


สาขาวิชาเคมี ภาควิชาเคมี

คณะวิทยาศาสตร์ จุฬาลงกรณ์มหาวิทยาลัย

ปีการศึกษา 2550

ลิขสิทธิ์ของจุฬาลงกรณ์มหาวิทยาลัย

MOLECULAR DYNAMICS OF M2 CHANNEL PROTEIN OF INFLUENZA A VIRUS



Miss Chittima Laohpongspaisan

สถาบันวิทยบริการ
จุฬาลงกรณ์มหาวิทยาลัย

A Dissertation Submitted in Partial Fulfillment of the Requirements
for the Degree of Doctor of Philosophy Program in Chemistry

Department of Chemistry

Faculty of Science


Chulalongkorn University

Academic year 2007

Copyright of Chulalongkorn University

Thesis Title MOLECULAR DYNAMICS OF M2 CHANNEL PROTEIN OF
INFLUENZA A VIRUS
By Miss Chittima Laohpongspaisan
Field of Study Chemistry
Thesis Advisor Professor Supot Hannongbua, Dr. rer. nat.
Thesis Co-advisor Assistant Professor Pornthep Sompornpisut, Ph. D.

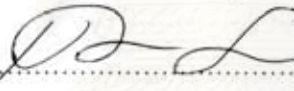
Accepted by the Faculty of Science, Chulalongkorn University in Partial Fulfillment of the
Requirements for the Doctoral Degree

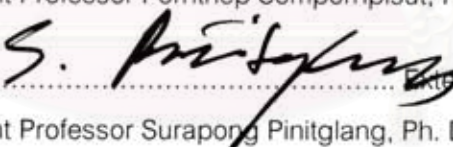

..... Dean of the Faculty of Science
(Professor Supot Hannongbua, Dr. rer. nat.)


THESIS COMMITTEE



..... Chairman
(Associate Professor Sirirat Kokpol, Ph. D.)


..... Thesis Advisor
(Professor Supot Hannongbua, Dr. rer. nat.)


..... Thesis Co-advisor
(Assistant Professor Pornthep Sompornpisut, Ph. D.)


..... External Member
(Assistant Professor Surapong Pinitglang, Ph. D.)


..... Member
(Professor Yong Poovorawan, M. D.)


..... Member
(Associate Professor Vudhichai Parasuk, Ph. D.)


..... Member
(Assistant Professor Somsak Pianwanit, Ph. D.)

จิตติมา เกาห์พงศ์ไพศาล: พลวัตเชิงโมเลกุลของโปรตีนเอ็ม-2 แชนแนลของไวรัสอินฟลูเอนซาเอ.

(MOLECULAR DYNAMICS OF M2 CHANNEL PROTEIN OF INFLUENZA A VIRUS)

อ. ที่ปรึกษา: ศ. ดร.สุพจน์ หารหนองบัว, อ. ที่ปรึกษาร่วม: ผศ. ดร. พรเทพ สมพรพิสุทธิ์, 77 หน้า.

โปรตีนเมทริกซ์-2 (เอ็ม-2) จากเชื้อไวรัสอินฟลูเอนซาเอ เป็นอินทิกรัลเมมเบรนไอออนแชนแนลชนิดหนึ่งที่มีบทบาทสำคัญในกระบวนการเพิ่มจำนวนของเชื้อไวรัส เนื่องจากการแพร่ระบาดของโรคไข้หวัดนกและการคือยาของเชื้อไวรัสสายพันธุ์ H5N1 โปรตีนเอ็ม-2 จึงได้กลายมาเป็นเป้าหมายสำคัญในการพัฒนาวัคซีนต้านเชื้อไวรัส การจำลองพลวัตเชิงโมเลกุลของทรานสเมมเบรนโดเมนของเอ็ม-2 แชนแนลถูกนำมาใช้เพื่อวิเคราะห์สมบัติเชิงโครงสร้างและเชิงพลวัตที่เกี่ยวข้องกับกลไกการส่งผ่านโปรตอน การทำงานระดับโมเลกุลของโปรตีนนี้ขึ้นอยู่กับกรดอะมิโนฮิสติดีนของแชนแนลทหระเมอร์ซึ่งทำหน้าที่เหมือนประตูสำหรับการส่งผ่านโปรตอนผ่านเมมเบรนไบเลเยอร์ สำหรับการศึกษาได้สร้างแบบจำลองของระบบที่ประกอบด้วยสภาวะโปรโตเนชันที่เป็นไปได้ทุกสภาวะของฮิสติดีน-37 โดยกำหนดประจุที่วงอิมิดาโซลทั้งสี่ขั้วยูนิตเท่ากับ 0 จนถึง +4 โมเดลทั้ง 6 ที่ศึกษานี้สอดคล้องกับสภาวะนอน, โมโน, ได (สับยูนิตที่อยู่ติดกันและทแยงมุมกัน) ไตร และเตตระโปรโตเนชัน ผลการทดลองแสดงให้เห็นว่าน้ำสามารถผ่านแชนแนลได้ยกเว้นสภาวะนอน, โมโนและไดโปรโตเนชัน นอกจากนี้ ได้ใช้วิธีพลวัตเชิงโมเลกุลศึกษาการยึดจับกับอะมันทาดีนและริมันทาดีนซึ่งเป็นสารอุดช่องแชนแนลผลของซิมูเลชันชี้ว่ามีตำแหน่งการยึดจับกับยาที่น่าจะเป็นไปได้สองตำแหน่ง ได้แก่กรดอะมิโนบริเวณปลายด้านนอกเซลล์ และภายในช่องของแชนแนล นอกจากนี้ริมันทาดีนแสดงประสิทธิภาพการยับยั้งการส่งผ่านน้ำที่สูงกว่าอะมันทาดีนซึ่งผลการยับยั้งที่ได้จากซิมูเลชันสอดคล้องกับผลทางการทดลอง สำหรับหัวข้อสุดท้ายของการศึกษานั้น ได้ทำการจำลองพลวัตเชิงโมเลกุลของแชนแนลกลายพันธุ์ที่คือยา โดยศึกษาแชนแนลที่มีการเปลี่ยนกรดอะมิโนเพียงตำแหน่งเดียวจำนวน 3 ชนิด คือ S31N, A30T, และ L26I เพื่อให้เข้าใจกลไกระดับโมเลกุลของการยึดจับกับยาและการคือยา จากผลศึกษาชี้ให้เห็นว่า อะมันทาดีนให้ฤทธิ์ทางชีวภาพที่ไม่ดีในระบบที่มีสภาวะไตรโปรโตเนชันของแชนแนลกลายพันธุ์ชนิด A30T ในขณะที่ระดับการคือยาต่ออะมันทาดีนของ L26I มีค่าสูงกว่า S31N


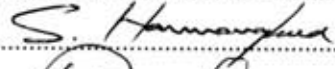
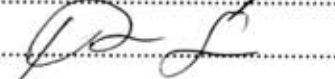
ภาควิชา.....เคมี..... ลายมือชื่อนิสิต.....
 สาขาวิชา.....เคมี..... ลายมือชื่ออาจารย์ที่ปรึกษา.....
 ปีการศึกษา..... 2550..... ลายมือชื่ออาจารย์ที่ปรึกษาร่วม.....

4673803323 : MAJOR CHEMISTRY

KEY WORD: INFLUENZA A M2 / BIRD FLU / MOLECULAR DYNAMICS / M2 PROTON CHANNEL / AMANTADINE

CHITTIMA LAOHPONGSPAISAN: MOLECULAR DYNAMICS OF M2 CHANNEL PROTEIN OF INFLUENZA A VIRUS. THESIS ADVISOR: PROF. SUPOT HANNONGBUA, Dr. rer. nat. THESIS COADVISOR: ASST. PROF. PORNTHEP SOMPORNPIST, Ph. D., 77 pp.

The matrix protein 2 (M2), an integral membrane ion channel from influenza A virus, plays an essential role in the viral replication process. Due to the emergence of bird flu disease and the drug resistant strain of H5N1, the M2 channel has become an important target for anti-flu drug development. Molecular dynamics (MD) simulations of the proton-selective transmembrane M2 channel in fully hydrated phospholipid bilayer were carried out to investigate structural and dynamic properties underlying the proton transport mechanism. Molecular mechanism of protein function relies on the histidine residues of the tetrameric channel, acting like the gate for transport of a proton through membrane bilayer. For this study, all possible protonation states of the ionizable His37 were constructed to have neutral and positively charged imidazole up to +4. The six studied models correspond to non-, mono-, di- (at adjacent and diagonal subunit), tri- and tetraprotonation states. The results show that except for non- and di -protonation states at adjacent position, the transport of water molecule across the channel was observed. In addition, the binding of amantadine and rimantadine, the channel blocker, were also assessed by MD simulation approach. MD results suggested two potential binding sites for the drugs, *i.e.*, the residues near the extracellular mouth and inside the inner cavity of the channel pore. Moreover, rimantadine showed the blocking activity of the water transport more efficient than amantadine. This biological activity of the drugs agrees well with experimental data. For the last topic of the thesis, MD simulations of the drug resistant M2 mutants were performed. Three single mutants including S31N, A30T, and L26I were studied to gain insight into molecular mechanisms of drug binding and resistance. The results indicated that in tri-protonation state amantadine loses its function in the A30T mutant while the degree of resistance to amantadine in the L26I mutant is higher than that in the S31N mutant.

Department.....Chemistry.....	Student's signature..... 
Field of study.....Chemistry.....	Advisor's signature..... 
Academic year.....2007.....	Co-advisor's signature..... 

CONTENTS

ABSTRACT IN THAI	iv
ABSTRACT IN ENGLISH	v
ACKNOWLEDGEMENTS	vi
CONTENTS	vii
LIST OF TABLES	x
LIST OF FIGURES	xi
CHAPTER I INTRODUCTION	1
1.1 Outbreak and Crisis of Influenza Virus	1
1.2 Historical Outline and the Lesson from past pandemics.....	1
1.3 Genetic variation of influenza A virus	2
1.4 Drug targets for anti-flu.....	4
1.5 M2 proton channel.....	6
1.6 Inhibition of the proton-transport M2 channel by Amantadine.....	8
1.7 Drug-target interactions.....	9
1.8 Objectives of this study.....	11
CHAPTER II Theory of Molecular Dynamics Simulations	12
2.1 Molecular Dynamics Simulation	12
2.1.1 Integration Algorithms	14
2.1.2 The LINCS algorithm.....	14
2.1.3 Periodic boundary conditions.....	15
2.1.4 Cutoff.....	16
2.1.5 Phase space & Ensembles.....	17
2.1.6 The ergodic hypothesis.....	18
2.2 Analysis from MD results.....	19
2.2.1 The root mean square deviations.....	19
2.2.2 The hydrogen bond.....	20
2.2.3 Radial Distribution Function.....	20

CHAPTER III MD simulations of wild-type M2 Channel.....	22
3.1 Introduction	22
3.2 Methods.....	23
3.2.1 Sequence Alignment and Homology model.....	23
3.2.2 Construct an initial model.....	24
3.2.3 Setup of membrane/protein systems	26
3.2.4 NPT MD simulation of the M2 channel in POPC bilayer..	26
3.2.5 Computational Details.....	27
3.3 Results and Discussion	28
3.3.1 Structural Stability of M2-Channel	28
3.3.2 Structural Properties of M2-Channel: Pore size.....	29
3.3.2.1 Distances between the backbone	
of the diagonal subunit: the rigid part.....	29
3.3.2.2 Distances between terminal side-chain of	
diagonal subunit: the flexible part.....	30
3.3.3 Characteristic of the Gating:	31
3.3.3.1 Side chains translating.....	31
3.3.4 Water Transportation through M2 Channel	31
3.3.4.1 Binding of water molecule to	
the selectivity filter residues.....	31
3.3.4.2 Atomic Density Profile.....	36
3.4 Conclusion.....	38
CHAPTER IV MD simulations of wild-type M2 channel-inhibitor complexes	39
4.1 Introduction.....	39
4.2 Methods.....	40
4.2.1 Construct an initial model.....	40
4.2.2 Setup of membrane/protein systems.....	41
4.2.3 MD Simulation details:.....	41
4.3 Results and Discussion:	42
4.3.1 Blocking of water transport.....	42
4.3.2 Inhibitor-solvent interaction.....	45

4.3.3 Mobility of the inhibitor in the M2 channel.....	47
4.3.4 Inhibitor binding site in the M2 channel.....	49
4.3.5 Orientation of Inhibitor in M2 channel.....	52
4.4 Conclusions.....	54
CHAPTER V MD simulations of mutant M2 channel-inhibitor complexes: a study of drug resistance to amantadine.....	56
5.1 Introduction.	56
5.2 Methods	56
5.2.1 Construct initial model of M2 mutants and their complexes...	56
5.2.2 Molecular dynamics simulations.....	57
5.3 Results and Discussion... ..	58
5.3.1 Effects of the single mutant of M2 protein on its functional machinery.....	58
5.3.3 Solvation of Amantadine (H-Bond with Water).....	64
5.4 Conclusions.....	65
CHAPTER VI Conclusions.....	66
6.1 MD simulations of drug-free M2 channel.....	66
6.2 Simulations of wild-type M2 complexed with amantadine or rimantadine.....	66
6.3 Simulations of MT-M2 complexes with amantadine.....	67
6.4 Suggestion for further work.....	67
REFERENCES.....	68
BIOGRAPHY.....	77

LIST OF TABLES

Table 1.1 The known flu pandemics in the last century.....	3
Table 1.2 Cumulative number of confirmed human cases of avian Influenza A (H5N1) reported to WHO until 11 March 2008.....	3
Table 5.1 The percent of H-bond (0, 1, 2, and 3) between drug and water for 0H and 3H states of three M2 mutants.....	64



สถาบันวิทยบริการ
จุฬาลงกรณ์มหาวิทยาลัย

LIST OF FIGURES

Figure 1.1 Area reporting the occurrence of H5N1 in poultry and wild birds since 2003.....	2
Figure 1.2 Diagram of influenza nomenclature.....	4
Figure 1.3 The replication cycle of Influenza virus.....	5
Figure 1.4 The native (97-residue) M2 protein consists of 3 domains: 24-residue N-terminal extracellular sequence, 19-residue transmembrane (TM) domain, 54-residue cytoplasmic tail.....	7
Figure 2.1 A two-dimensional array of box, as molecule 1 moves from the central box into box B it is replaced by its image which moves from box F into the central box. This movement is replicated across all the boxes.....	16
Figure 2.2 (a) criterion of H-bond geometry between two molecules and (b) H-bond bridges through water molecule.....	20
Figure 2.3 definition of $g_{AB}(r)$ according to the equation 2.24.....	21
Figure 3.1 Basic biochemical properties of the M2 protein channel	23
Figure 3.2 The sequence alignment of full-length M2 protein.....	25
Figure 3.3 The sequence alignment of TM-M2 domain, H3N2, H5N1 and H1N1.....	26
Figure 3.4 (a) top view of schematic representation of the TM-M2, (b) side view of whole system of M2 embedded in equilibrated lipid bilayer (POPC) (c) side view where the His37 and Trp41 residues were zoomed.	27

Figure 3.5 Average RMSD of entire backbone protein compare to the initial structure in the five simulated states (0H-black, 1H-red, 2Ha-green, 2Hd-blue, 3H-purple, and 4H-cyan) versus the simulation time...	28
Figure 3.6 Distances between the diagonal His37 and Trp41 residues, measured from C^α of the i^{th} and j^{th} subunits, RC^α -His37 $_{i,j}$ and $R C^\alpha$ - Trp41 $_{i,j}$ (see also Figure 3.4c) extracted from the MD trajectories of the six simulated systems (0H, 1H, 2Ha, 2Hd, 3H and 4H).....	29
Figure 3.7 Distances between the diagonal i^{th} and j^{th} subunits measured from the N-epsilon (N^ϵ) of His37 and C^h (CH) of Trp41, $R N^\epsilon$ -His37 $_{i,j}$ and RCH - Trp41 $_{i,j}$ (see also Figure 3.4c) for the six simulated systems (0H, 1H, 2Ha, 2Hd, 3H and 4H).	30
Figure 3.8 The average torsion angles of the four subunits of the His37 (a) and Trp41 (b) side chains.....	32
Figure 3.9 (a) RDF average of six systems 0H, 1H, 2Ha, 2Hd, 3H, and 4H, respectively. (A) and (B) average RDF at region of nonprotonated- N^δ and N^ϵ at the same subunit, (C) and (D) average RDF at region of protonated- N^δ and N^ϵ at the same subunit. (b) Schematic representation of His37 tetrad where the numbers are water in each region.....	34
Figure 3.10 Density profiles of each component in five systems were plotted along box size (\AA).....	36
Figure 3.11 Snapshots of five states were represented with space-filled of Water molecules.....	37
Figure 4.1 Adamantane derivatives of M2 inhibitors.....	39

Figure 4.2 Schematic of M2 channel and its inhibitors (A) Side view of the M2 channel with Ala30, Ser31, His37 and Trp41 residues, (B) top view of the M2 protein channel, and (C) the two inhibitors, where the distance scale L was used for the density plot shown in Figure 2. $L = 14 \text{ \AA}$ and $L = 50 \text{ \AA}$ denote coordinates of the ends of the N- and C-terminals, respectively..... 40

Figure 4.3 Water density along the M2 channel (see Figure 4.2 for the definition of the distance L) for free M2 and its complexes with amantadine and rimantadine in the 6 protonation states (0H, 1H, 2Ha, 2Hd, 3H and 4H), where the filled areas (magenta for amantadine and dark cyan for rimantadine) represent distributions of the inhibitor's coordinates along the channel and the vertical dashed lines indicate average positions of the four Ala30 and four His37..... 44

Figure 4.4 Radial distribution functions, $g(r)$. Plots of $g(r)$ from nitrogen atoms of amantadine (magenta) and rimantadine (dark cyan) to oxygen atoms of water. First-shell coordination numbers integrated up to the first minimum (marked by an arrow) are indicated..... 46

Figure 4.5 Density of M2 inhibitor center of mass. Frequency (vertical axis) of center of mass locations from the ten simulated systems of (A) amantadine and (B) rimantadine projected onto the square (xy-plane) formed by the four C_{α} atoms (represented by cylindrical tubes) of the histidine tetrad..... 48

Figure 4.6 Hydrogen bond occupations between M2 residues and inhibitors The hydrogen bond occupation between M2 residues and the inhibitors amantadine (magenta) and rimantadine (dark cyan) for the eight simulated systems, where I-IV denote the four units of the M2 protein tetrad..... 51

Figure 4.7 Orientation of the inhibitors. (A) Distribution of the angle θ , defined in (B) by 2 vectors, of which one points along the C-X bond (where X=N and C for amantadine and rimantadine, respectively) and the other points parallel to the M2 channel from the N- to the C-terminal (see text for details).....	53
Figure 4.8 Position and orientation of inhibitors in M2 channel. Sketches showing the position and orientation of (a) amantadine and (b) rimantadine as summarized from Figures 4.3, 4.5, 4.6 and 4.7 (see text for details).....	55
Figure 5.1 (a) The system box where the distance scale L was used for the density plot shown in Figure 5.1, $L = 14 \text{ \AA}$ and $L = 50 \text{ \AA}$ denote coordinates of the ends of the N- and C-terminal and the amantadine was zoomed into stick and ball. (b) Three single M2 mutants, L26I, A30T, and S31N.....	58
Figure 5.2 Water density along the three single mutant M2 channels (see Figure 1 for the definition of the distance L). Two protonation states (0H and 3H) of MT-M2s (S31N, A30T, L26I) complexed with amantadine are shown where the filled magenta area represents the distribution of the amantadine along the channel and the vertical dashed lines indicate Ala30 and His37. The first row shows the results of WT complexed with drug (black line) and Free M2 (gray line) (RF represents the resistant fold value of amatadine-resistance mutants compared to WT-M2 strain).....	59
Figure 5.3 Hydrogen bond occupations between three MT-M2 residues and amantadine The hydrogen bond occupation between residues of MT-M2 and drug for six simulated systems, where I-IV denote the four subunit of MT-M2 protein tetrad.....	63

CHAPTER 1

INTRODUCTION

1.1 Outbreak and crisis of influenza virus

Influenza pandemics and their worldwide epidemics have devastated uncountable people in history until now[1-4]. The Influenza A virus has caused substantial morbidity and fatality in humans and animals including the economics[5-7]. Recently, highly pathogenic avian influenza virus, H5N1, has caused diseases outbreaks which have a significant impact on the global economy and industry by large-scale death of poultry, subsequent infection and death in human over 200 people since 2003 (see Figure 1.1)[2, 3, 8]. Furthermore, distribution of genetic mutations associated with resistance to the M2 ion channel blocking adamantane derivatives among H5N1 isolated in Asia (Table 1.2)[8, 9]. The preparedness for treatment caused by currently circulating H5N1 viruses has been recommended by World Health Organization. The concern of vaccine, in the absence of an effective drug, might not be enough in quantities sufficient to counter this virus if it mutates to cause human-to-human transmission and would rely largely on the prophylactic and therapeutic properties of antiviral treatment.

An important and growing problem of resistance to anti-influenza virus drugs calls for the need to eventually develop more effective therapies for this viral subtype[10, 11]. Computer simulations method, one in various ways to solve such problems for improvement and development of the available anti-influenza drugs is currently needed[5, 6, 12-14].

1.2 Historical outline and the lesson from past pandemics

The word influenza has originated since 15th century in Italy where the disease was attributed (ascribed) to unfavorable astrological influences. The development in medical thought led to modify to *del freddo*, meaning “influence of the cold”[15]. The term influenza was first used in English in 1743 during an outbreak of the disease in Europe. The symptoms of influenza virus have described for a long time by Hippocrates roughly 2400 years ago (412 B.C.) in which what is difficult to interpret. Due to the symptoms are similar to others diseases, such as diphtheria, pneumonia,

typhoid, fever, dengue, or typhus. However, the influenza pandemic was firstly recorded of an outbreak in 1580, which began in Asia and spread to Europe via Africa. Pandemics continued sporadically throughout until the most famous and lethal outbreak, so-called Spanish flu (see Table 1.1)[15]. Later flu pandemics, Asian flu and Hong Kong Flu, were not so devastating. Even these were small outbreak they killed the millions of people.

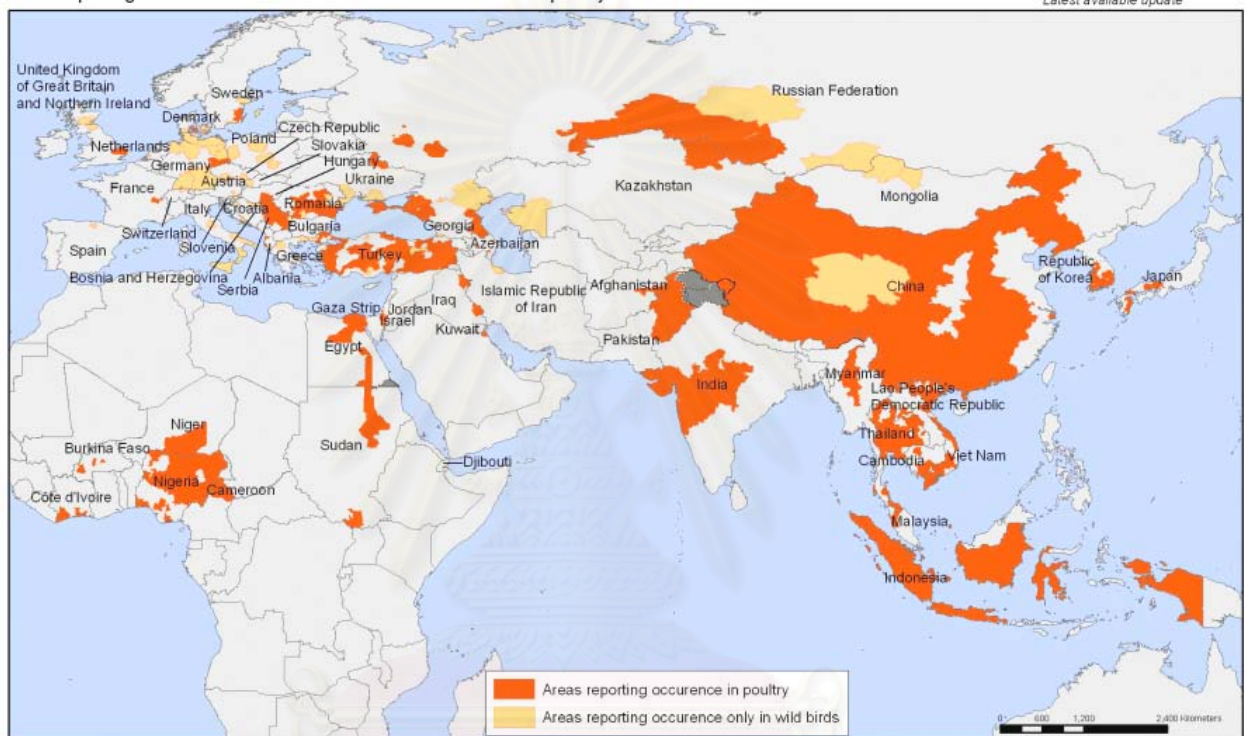


Figure 1.1 Area reporting the occurrence of H5N1 in poultry and wild birds since 2003[16].

1.3 Genetic variation of influenza A virus

Influenza A virus, commonly known as flu, is infectious disease of birds, mammals, and human caused by an RNA virus belonging to the family Orthomyxoviridae (Influenza virus). The natural hosts for the multi-variation of influenza A viruses are wild birds. Occasionally, viruses are transmitted into other species and may then cause devastating outbreaks in domestic poultry including humans. In humans, common symptoms of influenza infection are fever, sore throat, muscle pains, severe headache, coughing, weakness and fatigue.

The virus is able to cause both annual winter epidemics of varying size and severity, and occasional more severe pandemics. It can alter gradually through the process of random mutation, *antigenic drift*, every few years it will be result a significant epidemics. It may also change abruptly, *antigenic shift*, leading to a new subtypes and causing pandemic.

Table 1.1 The known flu pandemics in the last century[17].

Flu	Year	Deaths/million(s)	Subtype Involved
Spanish	1918	40-100	H1N1
Asian	1957	1	H2N2
Hong Kong	1968	1	H3N2

Table 1.2 Cumulative number of confirmed human cases of avian Influenza A (H5N1) reported to WHO until 11 March 2008[18].

Country	2003		2004		2005		2006		2007		2008		Total	
	cases	deaths	cases	deaths	cases	deaths	cases	deaths	cases	deaths	cases	deaths	cases	deaths
Azerbaijan	0	0	0	0	0	0	8	5	0	0	0	0	8	5
Cambodia	0	0	0	0	4	4	2	2	1	1	0	0	7	7
China	1	1	0	0	8	5	13	8	5	3	3	3	30	20
Djibouti	0	0	0	0	0	0	1	0	0	0	0	0	1	0
Egypt	0	0	0	0	0	0	18	10	25	9	4	1	44	19
Indonesia	0	0	0	0	20	13	55	45	42	37	12	10	129	105
Iraq	0	0	0	0	0	0	3	2	0	0	0	0	3	2
Lao	0	0	0	0	0	0	0	0	2	2	0	0	2	2
Myanmar	0	0	0	0	0	0	0	0	1	0	0	0	1	0
Nigeria	0	0	0	0	0	0	0	0	1	1	0	0	1	1
Pakistan	0	0	0	0	0	0	0	0	1	1	0	0	1	1
Thailand	0	0	17	12	5	2	3	3	0	0	0	0	25	17
Turkey	0	0	0	0	0	0	12	4	0	0	0	0	12	4
Viet Nam	3	3	29	20	61	19	0	0	8	5	4	4	105	51
Total	4	4	46	32	98	43	115	79	86	59	23	18	369	234

The influenza A viruses can be subdivided into different serotypes according to antibody responding to these viruses or they are divided into subtypes based on two

proteins on the surface of the virus: hemagglutinin, (HA) and the neuraminidase (NA). There are 16 different hemagglutinin subtypes and 9 different neuraminidase subtypes, all of which have been found among influenza A viruses in wild birds. Such serotypes which have caused the known human pandemics are as follow: H1N1 caused “Spanish Flu”, H2N2 caused “Asian Flu”, H3N2 caused “Hong Kong Flu”, H5N1 is a pandemic threat since 2003, H7N7 has unusual zoonotic potential, H1N2 is endemic in humans and pigs and so on. The name of viruses can be classified by type of virus, geographic origin, strain, and subtype (see Figure 1.2).

Wild birds are the primary natural reservoir for all subtypes of influenza A viruses and are thought to be the source of influenza A viruses in other animals and human. M2 is a minor component of virions, but is abundantly expressed on the plasma membrane of infected cells. It regulates the proton transport across cell membranes with high efficiency and selectivity.

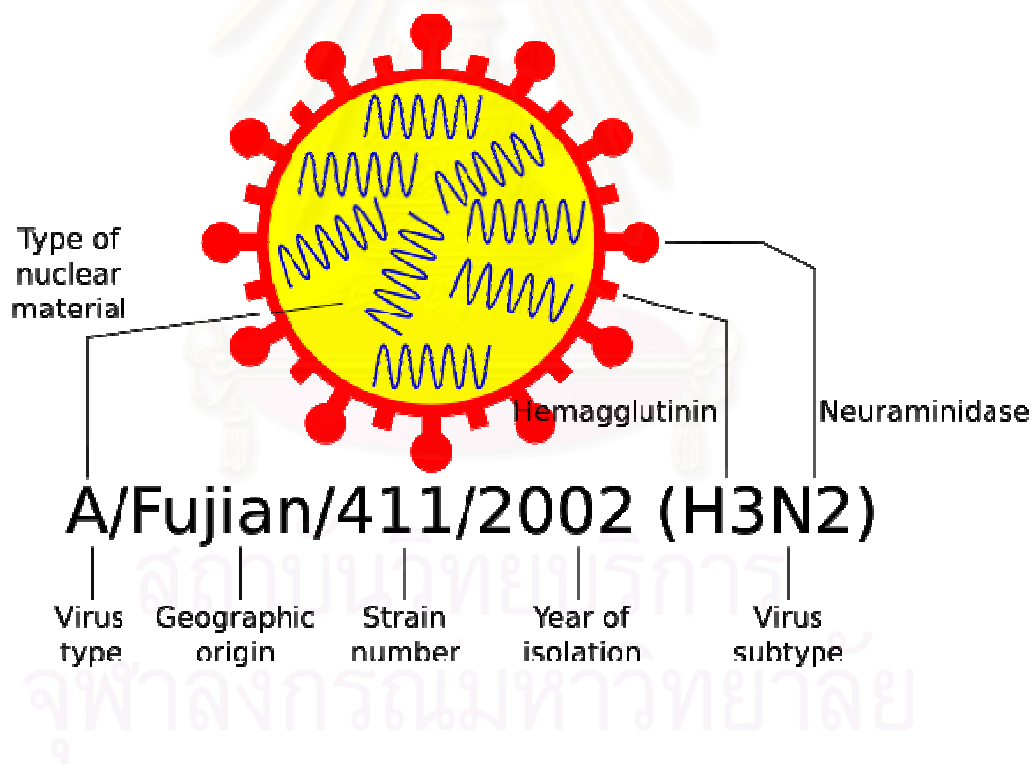


Figure 1.2 Diagram of influenza nomenclature[17].

1.4 Drug targets for anti-flu

The life cycle of influenza virus shows in Figure 1.3. Firstly, influenza A virus HA binds to a sialic acid receptor on the surface membrane of the infected membrane. Influenza viruses enter the infected cells through receptor-mediated endocytosis.

While in the acidic endosome, HA protein undergoes a conformational change to its low pH form that exposed to a hydrophobic fusion peptide, and after fusion the interior of virus is exposed to cytoplasm of infected cell. However, fusion alone is insufficient, for the release of the viral genetic material (uncoating), because the release of the ribonuclear proteins (RNPs) are only released from the matrix (M) at low pH . While the viruses are in the endosome, the M2 proton channels are activated by low pH and acidify the viral interior which consequently interrupts the interaction between the viral matrix proteins and ribonucleoproteins, a prerequisite process for uncoating (release of viral RNA into the cytoplasm). Besides its function in the uncoating process, the M2 proteins also modulate the pH between the acidic trans-Golgi network and the cytoplasm. The M2 protein extracted from influenza A virus is a 96 amino acid in length including a single transmembrane helix which forms proton-selective channels essential to virus function.

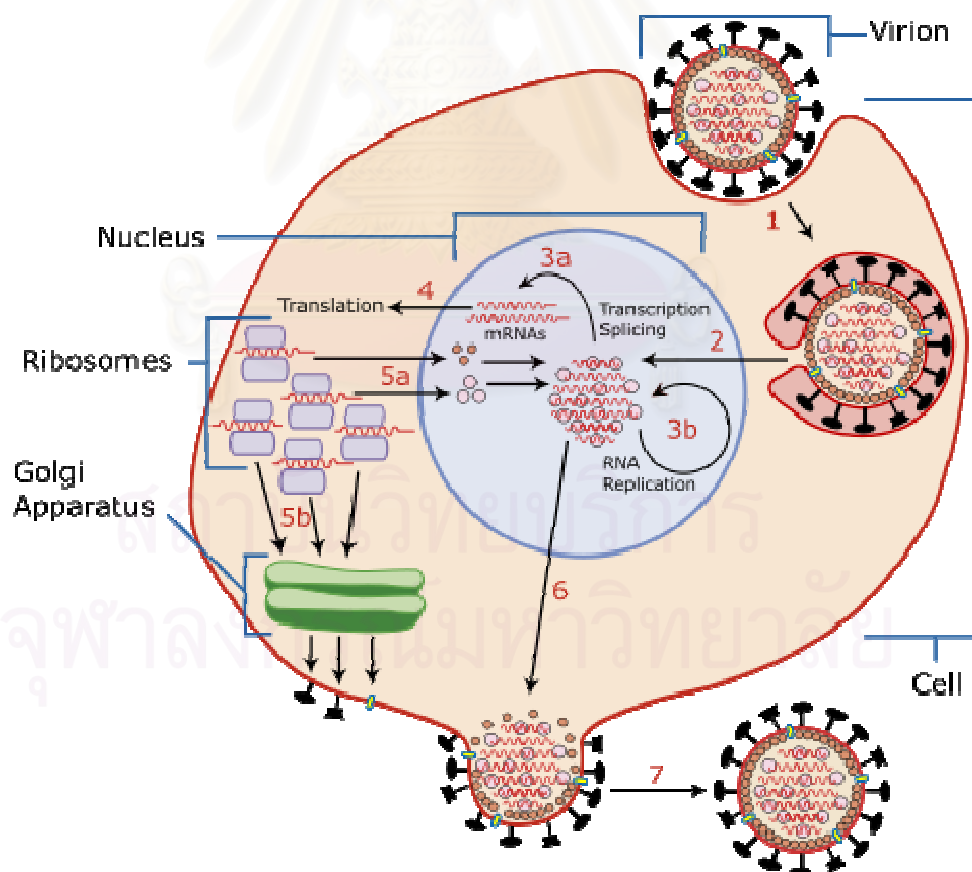


Figure 1.3 The replication cycle of Influenza virus[19].

1.5 M2 proton channel

The M2 ion channel is an integral membrane protein taking essential role in the life cycle of influenza A virus. The M2 protein is encoded by the spliced mRNA segment 7 of Influenza A virus, and includes a 24-residue N-terminal extracellular domain, a 19-residue hydrophobic transmembrane domain, and a 54-residue cytoplasmic tail[20, 21]. M2 forms a homotetrameric transmembrane α -helical bundle that acts as a H^+ channel. The main functional machinery of the M2 ion channel is believed to lie within the TM domain, *i.e.*, a synthetic 25-residue peptide (Ser-Ser-Asp-Pro25-Leu-Val-Val-Ala-Ala-Ser31-Ile-Ile-Gly-Ile-Leu-His37-Leu-Ile-Leu-Trp41-Ile-Leu43-Asp-Arg-Leu) spanning the TM domain exhibits proton channel activity similar to that of the full-length M2 protein (see Figure 1.4)[21-26].

M2 proton channel takes a role as pH modulators at two stages in the replication of viral life cycle. Viruses initially enter into cells via endocytosis *i.e.* the host cell engulfs a virus and then an endosome forms. In this acidic compartment ($pH = 5-6$), the opening of the M2 channel imports protons into the virion, triggering change in the proton-proton and protein-membrane interactions that leads to uncoating of viral particle. In the late stage of infection, a newly synthesized M2 proteins forms a channel in the trans Golgi network and balance the pH gradient across the membrane. In the latter case, the channel exports protons from trans Golgi lumen to the cytoplasm[20, 21, 25, 27-29]. To date, two competing hypotheses have been proposed. The two mechanisms, shuttle and gating mechanisms, however, differ substantially in the proposed ways in which protons navigate the gate formed by the histidine residues[30-33].

The channel is closed at physiological pH and is activated at $pH \leq 6.2$, a function attributed to the H37 residue located in the channel pore[34]. M2's H^+ channel activity is crucial to the virus life cycle in two aspects: First, following virus endocytosis and endosome acidification, M2 is activated and results in the concomitant acidification of the virus lumen. This acidification weakens the bonds between the viral RNA and the virus capsid[35]. Second, during viral exit, M2's channel activity ensures that the exosome does not acidify. This prevents the untimely, acid-triggered, irreversible conformational change of the viral hemagglutinin. Based on the above observations, it is obvious that any molecules that block the M2 channel would be an effective anti-influenza agent.

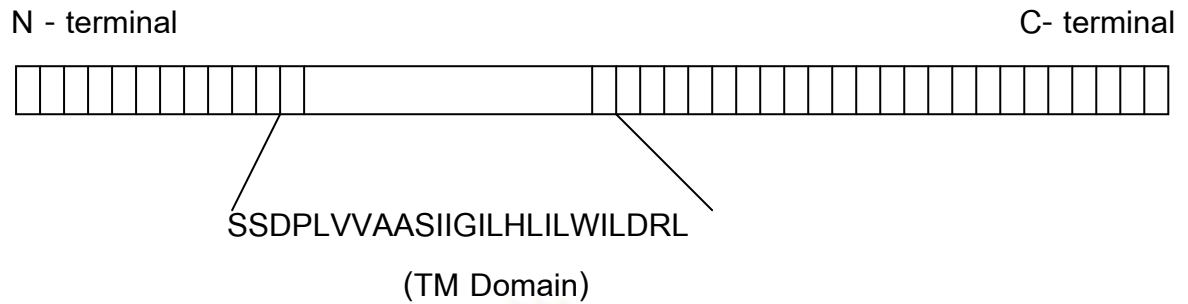


Figure 1.4 The native (97-residue) M2 protein consists of 3 domains: 24-residue N-terminal extracellular sequence, 19-residue transmembrane (TM) domain, 54-residue cytoplasmic (C-terminal) tail[24].

It is known that surface membrane proteins of the influenza virus A consist of three important components, hemagglutinin (HA), neuraminidase (NA), and M2 channels (see Figure 1.3). First, HA of Influenza A binds onto the sialic acid sugar importing the virus into acidic endosome of the host cell. Next, M2 takes main role as a *pH* mediate in uncoating viral genetics. Last, HA adheres, as before, to host when the mature virus buds off from the cell, NA has cleaved sialic acid residues from the host releasing the new influenza virus. The M2 channel is a proton-selective ion channel, a small integral membrane protein of the virus involved in the acid-induced process of uncoating the viral RNA during infection. It is a homotetrameric protein consisting of 97 residues per subunit. Each subunit comprises an extracellular N-terminal domain (24 residues), a transmembrane (TM) domain (19 residues), and an intracellular C-terminal domain (54 residues) (see Figure 1.4). The viral M2 protein functions as a proton selective channel which is activated by low pH environments as found in endosomes. The M2 channel allows protons to enter the interior of the viral particle, and this acidification dissociates the matrix protein M1 that coats the viral RNA genome, after which the viral genetic material can replicate[36].

1.6 Inhibition of the proton-transport M2 channel by Adamantane compound drugs.

Amantadine (1-aminoadamantane hydrochloride) and rimantadine (α -methyl-1-adamantane methylamine hydrochloride), an amantadine analogue, are commercial drugs used for the prophylaxis and treatment of influenza A by inhibiting the ion-channel activity of the M2 protein[13, 20, 21]. Amantadine is a specific anti-influenza A drug that inhibits viral replication, primarily by binding to the M2 channel and thereby preventing proton conductance[37-41]. Without the acidification of the viral interior, the uncoating process cannot be occurred. Although amantadine is effective in the prophylaxis and treatment of all influenza A subtypes, it has been associated with the central nervous system side effects. An increasing and persistent of resistance to adamantane on the animals and human has been frequently highlighted, especially in China and Hong Kong. The adamantane-resistant levels increase from below 10% during 1995-2002, rapidly growing to 58% in 2003, rising up to 74% in 2004, and finally being 92% during 2005-2006[5, 6]. The genetic analysis of drug-resistance emerging during treatment of influenza A virus showed that virus become resistant to adamantane through an amino acid substitution at the residues 26, 27, 30, 31 or 34 within the transmembrane region of M2 protein[7, 9, 42, 43]. The most common drug-resistance causes single mutation, but variants with double mutations have also been described.

The proton selectivity and channel gating are the key biological function of the M2 channel. This channel is highly proton selective at least 10^6 fold than other cations. The channel is low-*pH* gated, undergoing 50-fold conductance increase from *pH* 8.2 to *pH* 4.5. The detailed structure responsible for these functions remains unclear. There are, now, two proposed mechanisms for describing the transportation of proton along the M2 channel (during the proton uncoating), shuttle and gating mechanisms. Another one is for inhibition of M2 channel by inhibitor.

In the proton transport mechanisms, when the channel is activated, each histidine side chain accepts the excess proton to form a bi-protonated intermediate, which is presumed to be short-lived and tend to release either δ - or ϵ -hydrogen back to the pore water to become neutral again. The transport of a single proton through the gate is finished when the hydrogen at the opposite side is released to the

environment. Then, the initial state needs to be regenerated to transport the next proton which was hypothesized via tautomerization or just flipping of histidine imidazole. Another mechanism for proton transport, after the channel is activated, each of the histidine's side-chains can acquire an additional proton, and then become positively charged. And protons are not immediately released back to the pore water. Due to electrostatic repulsion between the positive charges, the histidine side chains, then, swing away from each other, the water penetrates through to form a continuous proton conductive water wire or proton wire. In this mechanism, the proton can be passed from one water molecule to another in the pore without water moving.

In the mechanism for inhibition of M2 channel by inhibitors, several lines of evidence point that the pore opening and closing is dependent on a single transmembrane domain residue, Trp41. There are two proposed mechanisms for inhibition by blocking with the inhibitor. The first is blocking at the residues at the mount region. Another one is to block at the histidine residue. However, the molecular mechanism for proton transport and opening channel of M2 are not fully understood.

1.7 Drug-target interactions

The homotetrameric M2 forms a proton selective ion channel activated at low *pH* and is the specific target of amantadine and rimantadine. It takes a role in the *pH* mediated-uncoating process of influenza virions during in endosomes. In addition, during infection by some subtypes (highly pathogenic influenza A virus) M2 is required to act as a proton-leak channel to elevate *pH* within trans-Golgi network preventing the premature acid activation of newly synthesized hemagglutinin.

A structural basis for M2-TM has been achieved by Fourier transform infrared spectroscopy[44], solid-state NMR spectroscopy[24, 45, 46], UV resonance Raman spectroscopy[47], electron spin resonance[48], cysteine mutagenesis[49], electrophysiological studies, and molecular dynamics simulations[23, 26, 50-54]. These suggest that the M2-TM residues Val27, Ala30, Gly34, His37, and Trp41 line the pore and, in addition, the imidazole side chain of His37 acts as a proton shuttle and interacts with the indole side chain of Trp41 to occlude the pore.

Molecular modeling studies of the M2 protein have been carried out, mainly, by two research groups[49, 54]. Early works were performed in vacuo, while the next

work tried to incorporate the effect of membrane environment using mimetic bilayer (octane slab solvated by water molecules), however the mimetic bilayer is not realistic for the sake of non polar head groups. To make this efficiency, more recent simulations of the M2 channel were performed in phospholipids membrane solvated by water molecules[33, 50, 55]. The modeling studies suggest that a column of water in the M2 channel can be interrupted only by the ring of His37 residues. The His37 acts as a molecular switch which allow water molecule, and hence proton, to move through the channel. In this study, different protonation states of histidine of M2 channel were investigated using molecular dynamics simulation to explore structural properties of the channel underlying the proton transport mechanism. Two proton mechanisms of M2 protein were proposed; shuttle mechanism[56] and gating mechanism[33].

Amantadine, the adamantane compound, was the first antiviral drug found to inhibit the replication of influenza A virus by blocking ion channel activity[40, 52] and has been used for over three decades. Amantadine and rimantadine are commercial drugs used for the prophylaxis and treatment of influenza A by inhibiting the ion-channel activity of the M2 protein[57-62]. However, the mechanism of how they interact with the M2 protein is still controversial. Conventionally, a hypothesis of inhibition invokes interactions of the drug with the mouth of the M2 pore, in which the inhibitor behaves as a 'blocker'[59, 63-65]. In this view, the adamantyl group interacts with Val24 and Ala27 via van der Waals interactions, while the charged amine group hydrogen bonds with Ser31. Alternatively, Pinto and co-workers proposed another model: that amantadine binds to a location deeper in the channel and its ammonium group hydrogen bonds with the His37 side chain[49, 66]. Binding of the drug is supposed to block proton channel activity by displacing water molecules that are essential for proton conduction. It may act as an allosteric inhibitor binding outside the pore region, which consequently leads to the conformation changes of the channel from the open state to closed state[20, 52, 67]. ¹H NMR spectroscopy data showed that amantadine interacted weakly with the liposomes, suggesting a mechanism by which it may first bind to the lipid bilayers and then block target channels after diffusion across the membrane surface[68]. Recently, ¹⁵N CPMAS NMR spectroscopy was used to study the effect of amantadine binding to the His37 side chain as a function of *pH*, implying a mechanism whereby amantadine interferes with the histidine facilitation of proton conductance[69]. Unlike the MS-

EVB simulation data combined with Poisson-Nernst-Planck (PNP) theory indicates that the triply protonated His37 state is the most likely open state with the estimated *pH* value of 5.5 from dielectric continuum theory[70]. This study views as being preliminary results that the Ala29 residue region is the primary binding site for the anti-flu drug amantadine in which it reduces the proton conductance by 99.8% due to a significant dehydration penalty of the excess proton in the vicinity of the channel-bound amantadine. However, the drug resistant viruses have rapidly emerged as a result of single mutation of amino acid at residue Leu26, Val27, Ala30, Ser31, Gly34 within transmembrane domain.

1.8 Objectives of this study

The study carried out molecular dynamics simulation approaches in order to address three important systems including the functional mechanism of the M2 in free form, the mechanism of drug inhibition and drug resistance in the wild-type and mutant M2 channel. In this thesis, the first two chapters 1 and 2 provide overviews of Influenza A and Theory of molecular dynamics simulations, respectively. Chapter 3, structure and dynamic properties of the wild-type M2 channel were investigated using molecular dynamics simulations in a fully hydrated lipid bilayer. Proton transport through the channel was discussed from the simulation of different protonation states of His37. In Chapter 4, molecular dynamics simulations of the wild-type M2 channel in the presence of anti-flu drugs, amantadine and rimantadine, were carried out to understand how drugs block the channel. This provides useful information for designing and discovering new and more potent inhibitors. Moreover, an important and growing problem of amantadine resistance has called the need for understanding in details how amantadine block proton transport. Thus, molecular dynamics study of the mutant M2 protein complexed with the two drugs was reported in Chapter 5. This is to seek for an answer why amantadine loses its functions in the mutant M2 proton channel.

CHAPTER 2

THEORY OF MOLECULAR DYNAMICS SIMULATIONS

Molecular dynamics (MD) simulations have been used to study a wide variety of biological applications, in which proteins share the largest part of the studied systems. During the last decades, membrane proteins have become a highly interesting topic as the 3D crystal structures of membrane proteins have been increasingly available. The MD technique has a great advantage by providing insight into the structure-function relationship at atomic levels.

MD is a simulation of time-dependent behavior of a molecular system. The MD technique is known as deterministic method, by which the state of system of the system at any future time can be predicted from its current state. It also represents an interface between laboratory experiments and theory, and can be understood as a “virtual experiment”.

2.1 Molecular Dynamics Simulation

Classical MD simulation[71] is relied on the second law of Newton’s equation of motion[72, 73]. The equation 2.1 describes the motion of a particle of mass m_i along the distance r_i with F_i being a force of the particle in that direction which can be defined as the second derivative of the position over time (equation 2.2) or the first derivative of velocities overtime (equation 2.3).

$$F_i = ma_i \quad (2.1)$$

$$\frac{d^2 r_i}{dt^2} = \frac{F_i}{m_i} \quad (2.2)$$

$$\frac{dv_i}{dt} = \frac{F_i}{m_i} \quad (2.3)$$

$$F_i = -\frac{\partial V}{\partial r_i} \quad (2.4)$$

The movement of the particle i in the system is governed by the force acting on it. The force acting on any atoms is computed by calculating the gradient of the potential energy (Equation 2.4). When the potential energy (V) of each interacting atoms is computed, forces are also obtained. From the force acting on atoms, it is possible to determine acceleration through the second law of Newton equation. An integration of such equation yields a trajectory describing how positions, velocities, and acceleration of the particles vary with time.

In protein simulations, the molecular mechanic (MM) empirical function is generally used to compute the potential energy of the systems. The MM potential energy computation consists of the two typical energy terms, the non-bonded and bonded energy (equation 2.5). The total potential energy is summed from contributions of bonded and non-bonded terms.

$$V(R) = \sum_{bonds} K_r (r - r_{eq})^2 + \sum_{angles} K_\theta (\theta - \theta_{eq})^2 + \sum \frac{V_n}{2} (1 + \cos[n\phi - \gamma]) + \sum_{i < j}^{atoms} \frac{A_{ij}}{R_{ij}^{12}} - \frac{B_{ij}}{R_{ij}^6} + \sum_{i < j}^{atoms} \frac{q_i q_j}{\epsilon R_{ij}} \quad (2.5)$$

where K_r, K_θ are stretching and bending force constants, r_{eq}, θ_{eq} are equilibrium values for bond-length and bond-angle, V_n is the rotational height, n is the periodicity of rotation, ϕ is torsional angle, γ is the phase angle, q exhibits point charges of atom i and j , ϵ is dielectric constant and R_{ij} is distance between atom i and j . The first three terms are used to calculate the bonded energy. The fourth term is the Lennard-Jones potential function and the last term is used to compute the coulombic energy.

In MD simulations, a series of configuration or trajectory that specifies how the positions and velocities of particles in the system vary with time is generated by integrating the Newton's laws of motion.

2.1.1 Integration Algorithms

In MD simulation, the force will change on each particle whenever the particle changes its positions. Under the influence of a continuous potential the motions of all particles are coupled together, giving rise to the many body problem that cannot be solved analytically. Therefore, a finite difference method has been applied to solve the equation of motion[72].

The movement of the atoms is simulated by numerically solving Newton's equation. The GROMACS MD program uses the leap-frog algorithm, the modified verlet algorithm, for integrating the equation of motion to update the time-step with Δt . This algorithm requires positions r at time t and velocities v at time $t - \frac{\Delta t}{2}$; it updates positions and velocities using the forces $F(t)$ determined by positions at time t :

$$v\left(t + \frac{\Delta t}{2}\right) = v\left(t - \frac{\Delta t}{2}\right) + \frac{F(t)}{m} \Delta t \quad (2.6)$$

$$r(t + \Delta t) = r(t) + v\left(t + \frac{\Delta t}{2}\right) \Delta t \quad (2.7)$$

$$r(t + \Delta t) = 2r(t) - r(t - \Delta t) + \frac{F(t)}{m} \Delta t^2 + O(\Delta t^4) \quad (2.8)$$

The leap-frog algorithm is of third order in r and time-reversible. As such merits, this algorithm can be compared with other time integration algorithms.

2.1.2 A Linear Constraint Solver for Molecular Simulations (LINCS)

algorithm

LINCS algorithm[72, 74] is used to reset bonds to their correct length after an unconstrained update according to the equation 2.9. It uses two steps. The first is the

projections of the new bonds on the old bonds which are set to be zero. In the second step, a correction is applied for improving the bonds.

$$\frac{d^2 r_i}{dt^2} = M^{-1} F \quad (2.9)$$

where F is $3N$ force vector and M is $3N \times 3N$ diagonal matrix, constraining the masses of the particles. The system is constrained by K time-independent constraint equations.

$$g_i(r) = |r_{i1} - r_{i2}| - d_i = 0 \quad i = 1, \dots, K \quad (2.10)$$

where the $g_i(r)$ is the generalized coordinates r .

2.1.3 Periodic boundary conditions

To simulate the system using relatively small number of particles and to decrease the edge effect in a finite system, the classical way is to apply periodic boundary condition [72, 73], *i.e.*, the atoms in simulated system are put to the space-filling box surrounded by translated copies of itself (Figure 2.2). The shape of space-filling unit cells for GROMACS is based on the triclinic unit cell. Combining the minimum image convention, the only one – the nearest – image of each particle is considered for short-range non-bonded interaction term. For long-range, GROMACS incorporates the lattice sum method like Ewald Sum, Particle Mesh Ewald (PME) Particle-Particle Particle Mesh (PPPM) methods. The electrostatic are totally given by equation 2.12.

$$V = \frac{f}{2} \sum_{n_x} \sum_{n_y} \sum_{n_z^*} \sum_i^N \sum_j^N \frac{q_i q_j}{r_{ij,n}} \quad (2.11)$$

where $(n_x, n_y, n_z) = n$, the box vector, the star points that term i equals j should be omitted. The range $r_{ij,n}$ is the real distance between charges excluding the minimum image. This equation is conditionally convergent, whereas it is very slow. Ewald summation is the improved method in which change the slowly converging into the quickly converging terms with a constant term. For other method, PME improves the performance of the reciprocal sum.

The box is defined by three vectors a , b , and c . It has to satisfy the following conditions:

$$a_y = a_z = b_z = 0 \quad (2.12)$$

$$a_x > 0, b_y > 0, c_z > 0 \quad (2.13)$$

$$|b_x| \leq \frac{1}{2}a_x, |c_x| \leq \frac{1}{2}a_x, |c_y| \leq \frac{1}{2}b_y \quad (2.14)$$

Equation 2.12 can be satisfied by rotating the box, while equations 2.13 and 2.14 by adding and subtracting box vectors[72].

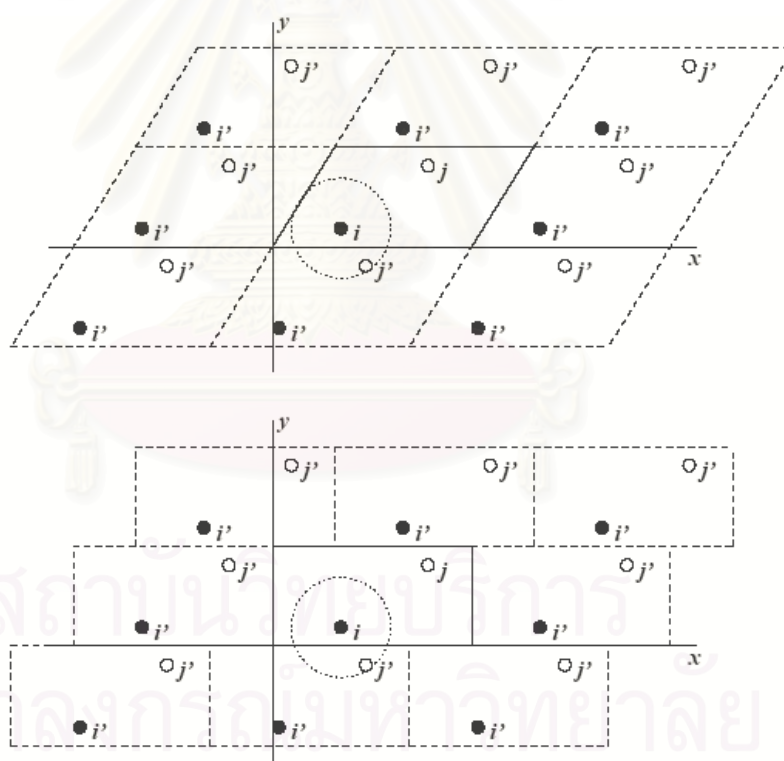


Figure 2.2

A two-

dimensional array of box, as molecule 1 moves from the central box into box B it is replaced by its image which moves from box F into the central box. This movement is replicated across all the boxes[72].

2.1.4 Cutoff

The most time-consuming part of simulation is the calculation of non-bonded energies of forces. The numbers of bonded terms are all proportional to the number of atoms, while the number of non-bonded terms is of order N^2 , represented by Lennard-Jones potential. The most popular way to deal with non-bonded interactions is to use non-bonded cut-off and to apply the minimum image convention[72].

The cutoff radius used to truncate non-bonded interactions must not exceed half of the shortest of box vector, $R_C < \frac{1}{2} \min(\|a\|, \|b\|, \|c\|)$, otherwise more than one image would be within the cutoff distance of the force.

2.1.5 Phase space & Ensembles

The state of a classical system can be completely described by specifying the positions and momenta of all particles[75]. The initial position can be obtained from experimentally resolved structures. The initial distribution of velocities is resolved from a Maxwell-Boltzmann distribution at given temperature see equation 2.15.

$$p(v_i) = \left(\frac{m_i}{2\pi k_B T} \right)^{\frac{1}{2}} \exp \left[-\frac{m_i v_i^2}{2k_B T} \right] \quad (2.15)$$

$$T = \frac{1}{(3N)} \sum \frac{|P|}{2m}$$

where $p(v_i)$ is the velocity probability density, N is number of atoms in the system, and p is momentum.

Space being three-dimensional, a particle is associated with six coordinates – a system of N particles is, then, characterized by $6N$ coordinates. The $6N$ -dimensional space defined by these coordinates is called ‘phase space’

Because phase space encompasses every possible state of a system, the average value of properties A at equilibrium (i.e., its expectation value) for a system having a constant temperature, volume, and number of particles can be written over phase space where P is probability of being at a particular phase point. From

statistical mechanics, we know that this probability depends on the energy associated with the phase point according to

$$P(q, p) = Q^{-1} e^{-E(q,p)/k_B T} \quad (2.16)$$

where E is the total energy, k_B is Boltzmann's constant, T is temperature, and Q is system partition function

$$Q = \iint e^{-E(q,p)/k_B T} dq dp \quad (2.17)$$

which may be thought of normalization constant for P .

2.1.6 The ergodic hypothesis

The experimentally value of properties, in general, depends upon the positions and momenta of particles that comprise the system written as $A(p^N(t), r^N(t))$, where $p^N(t)$ and $r^N(t)$ represent momenta and coordinates at time t of the N particles, respectively. Over time, the instantaneous value of property A fluctuates as a result of interaction between the particles[75]. The measured value is an average of A over the time of measurement known as *time average*. As the time over which measurement is increased to infinity, so the value of the following integral approaches the true average value of the property

System at 'reasonable' (i.e. low-energy) phase point, its energy conserving evolution over time, trajectory, seems likely relevant region of phase point. A reasonable way to compute a property average simply involving computing the value of properties periodically at times t , and assuming where M is the number of the property is sampled. In the limit of sampling continuously and following the trajectory indefinitely, this equation becomes

$$\langle A \rangle = \lim_{t \rightarrow \infty} \frac{1}{t} \int_{t_0}^{t_0+t} A(\tau) dt \quad (2.18)$$

The "ergodic hypothesis" assumes such a question to be valid and independent of choice of t_0 i.e. the ensemble average is equal to the time average.

To calculate the average values of the properties of the system, the dynamical behavior would be simulated determining values of $A(p^N(t), r^N(t))$ based on model of intra- and inter-molecular interactions.

The temperature (T) is given by the total kinetic energy of N -particle system:

$$E_{kin} = \frac{1}{2} \sum_{i=1}^N m_i v_i^2 = \frac{1}{2} N_{df} k_B T \quad (2.19)$$

where k_B is boltzmann's constant and N_{df} is the number of degrees of freedom computed from:

$$N_{df} = 3N - N_c - N_{com} \quad (2.20)$$

N_c is here the number of the constraints imposed on the system and N_{com} is additional degrees of freedom when performing molecular dynamics.

The pressure tensor (P) [73, 75] is calculated from the difference between kinetic energy E_{kin} and the virial Ξ

$$P = \frac{2}{V} (E_{kin} - \Xi) \quad (2.21)$$

where V is the volume of the computed box and the virial Ξ tensor is defined as

$$\Xi = -\frac{1}{2} \sum_{i < j} r_{ij} \otimes F_{ij} \quad (2.22)$$

2.2 Analysis from MD results

In this part, the trajectory, the production from molecular dynamics simulations, was obtained, and then analyzed in different way. Here, many properties were investigated by in-house code of Gromacs [71, 72] e.g. root mean square deviation, hydrogen bonding, inter-atomic distances, fluctuations of bond-angle and dihedral angle, density of each composition in the system and so on.

2.2.1 The root mean square deviations (RMSD)

RMSD of certain atoms in molecule with respect to a reference structure can be calculated by least-square fitting the structure to the reference.

$$RMSD(t_1, t_2) = \left[\frac{1}{M} \sum_{i=1}^N m_i \|r_i(t_1) - r_i(t_2)\|^2 \right]^{\frac{1}{2}} \quad (2.23)$$

where $M = \sum_{i=1}^N m_i$ and $r_i(t)$ is the position of atom i at time t .

2.2.2 The hydrogen bond (H-bonds)

H-bonds is determined between all possible H-bond donor (D) atoms and acceptor (A) atoms where distances $r \leq r_{HB} = 3.5 \text{ \AA}$ and angles $\alpha \leq \alpha_{HB} = 60^\circ$ (see Figure 2.2)[72].

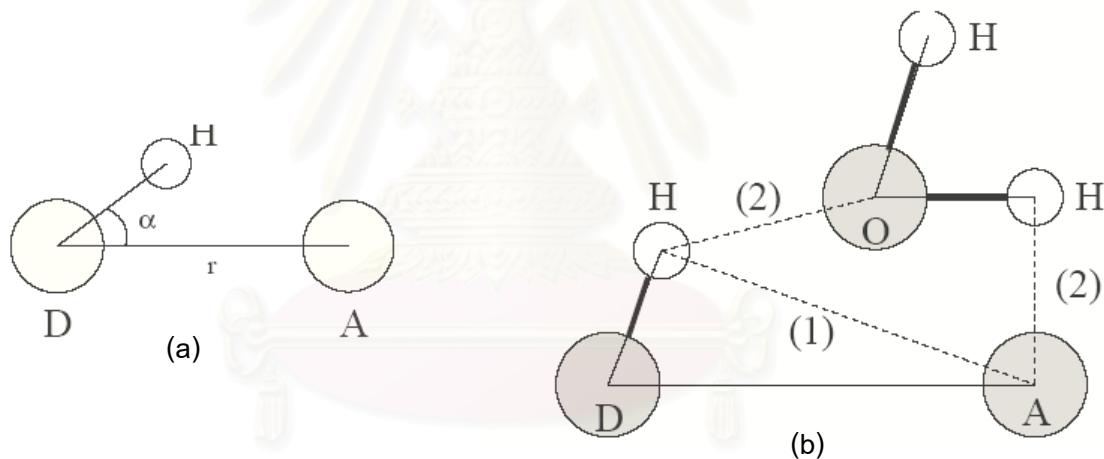


Figure 2.1 (a) criterion of H-bond geometry between two molecules and (b) H-bond bridges through water molecule.

2.2.3 Radial Distribution Function

The radial distribution function (*rdf*) can be defined as pair correlation functions $g_{AB}(r)$ between particles of type A and B. The *rdf* is expressed as

$$g_{AB}(r) = \frac{\langle \rho_B(r) \rangle}{\langle \rho_B \rangle_{local}} \quad (2.24)$$

It is a useful tool describing the structure of the system, particularly liquid and solid states.

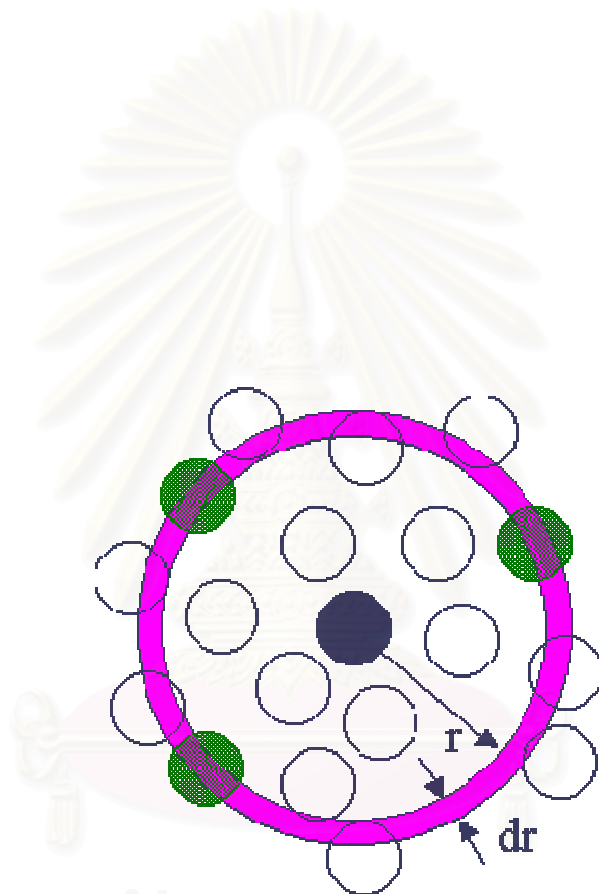


Figure 2.3 definition of $g_{AB}(r)$ according to the equation 2.24[72].

CHAPTER 3

MD SIMULATIONS OF WILD-TYPE M2 CHANNEL

3.1 Introduction

Although, the M2 channel is a homotetrameric protein consisting of 96 residues per subunit, the main functional machinery of the M2 ion channel is believed to lie within the transmembrane (TM) helical bundle (Figure 3.1). The TM domain contains approximately 25-residue long (Ser22-Ser-Asp-Pro-Leu-Val-Val-Ala-Ala-Ser-Ile-Ile-Gly-Ile-Leu-His37-Leu-Ile-Leu-Trp41-Ile-Leu-Asp-Arg-Leu), in which His37 plays an essential role for proton conduction. Structural studies achieved by Fourier transform infrared spectroscopy[44], solid-state NMR spectroscopy[24, 45, 46], UV resonance Raman spectroscopy[47], electron spin resonance[48] and cysteine mutagenesis[49] suggested that the M2-TM residues, Val27, Ala30, Gly34, His37, and Trp41 line the pore and, in addition, the imidazole side chain of His37 acts as a proton shuttle and interacts with the indole side chain of Trp41 to occlude the pore. To understand insight into structural and dynamical properties responsible for the protein function, molecular dynamics (MD) simulations of the wild-type M2 channel was performed in a fully hydrated lipid bilayer. Six different protonation states of the neutral or charged His37 were investigated using MD techniques in order to determine the most probable ionization states of the selectivity filter residues that change protein conformation from the closed to open states.

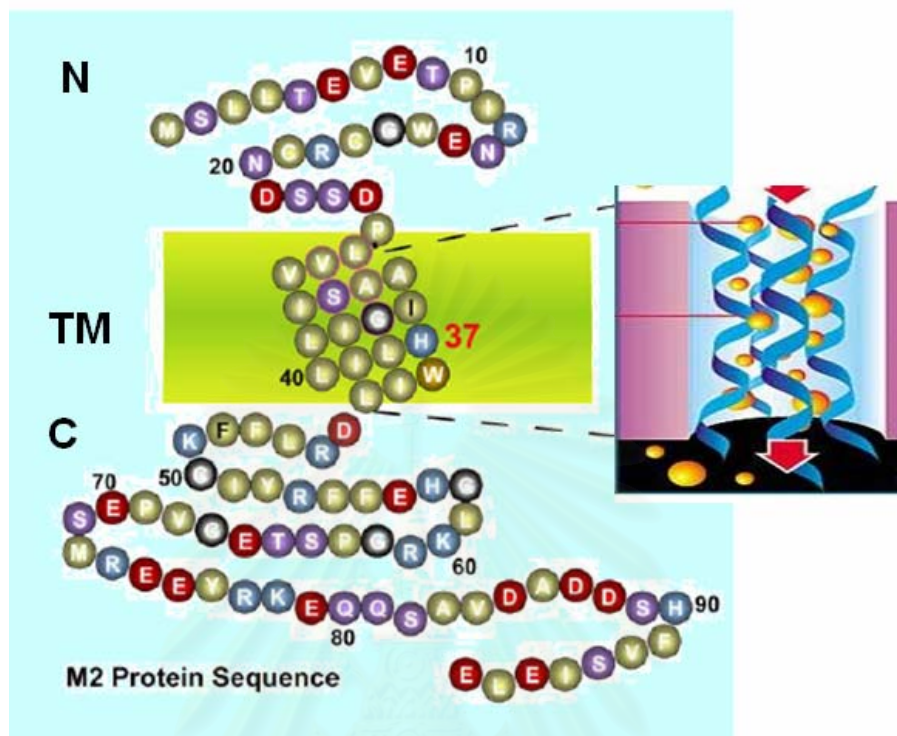


Figure 3.1 Basic biochemical properties of the M2 protein channel.

3.2 Methods

3.2.1 Sequence Alignment

All the M2 amino acid sequence used in the study was H3N2 stain taken from the genome database available in the National Center for Biotechnology Information (NCBI). Sequence comparison of the M2 protein from H5N1 virus with those from various subtypes of influenza A virus, including H5N2, H5N3, H2N2, H7N4, H3N6, H6N8, H7N9, H11N9, H6N1, H7N7, H7N2, H7N1, H9N2, H7N3, H6N2, H3N8, H1N1 and H3N2 was performed using Discovery Studio 1.7 software[76]. The sequence alignment is shown in Figure 3.2. The results show that the M2 sequences are highly conserved with sequence identity in a range of 90-98%. In particular, all the 25 residues in the transmembrane helix, of which 23 and 25 residues are identical to the M2 sequence of H1N1 (TW97), and H3N2 (Udorn72), respectively (Figure 3.3).

3.2.2 Construct an initial model

The 3D structure of the M2 channel is not yet solved by crystallographic or conventional NMR techniques. The M2 model available in the Protein Data Bank was derived based on solid-state NMR data and belongs to the H3N2 subtype only. Based on the sequence alignment of the transmembrane segment (Figure 3.2 and 3.3), the M2 sequence of H5N1 is identical to that of H3N2. Therefore, structural coordinates of the H5N1 M2 channel was constructed based on the available H3N2 model (1NYJ) without using homology[24].

The 3D structure of the M2 channel consists of four identical transmembrane helices (Figure 3.3). An arrangement of homotetrameric helical bundle forms the channel pore and adopts four folds symmetry relative to the channel axis. On the basis of ionizable His37 at N^ε, six protonation states were assigned for the study. They correspond to non-, mono-, di-, tri- and tetra- protonation states which are denoted as 0H, 1H, 2Ha, 2Hd, 3H and 4H, respectively. The 2Ha and 2Hd are considered as two protonated protons attached to His37 of adjacent and diagonal subunits, respectively.

	1	10	20																						
H3N2_Udorn72	S	S	D	P	L	V	V	A	A	S	I	I	G	I	L	H	L	I	L	W	I	L	D	R	L
H5N1_Goose	S	S	D	P	L	V	V	A	A	S	I	I	G	I	L	H	L	I	L	W	I	L	D	R	L
H5N1_chicken	S	S	D	P	L	V	V	A	A	S	I	I	G	I	L	H	L	I	L	W	I	L	D	R	L
H5N1_BlowFly	S	S	D	P	L	V	V	A	A	S	I	I	G	I	L	H	L	I	L	W	I	L	D	R	L
H1N1_TW97	S	S	D	P	L	V	V	A	A	S	I	I	G	I	V	H	L	I	L	W	I	I	D	R	L

Figure 3.3 The sequence alignment of TM-M2 domain, H3N2, H5N1 and H1N1.

3.2.3 Setup of membrane/protein systems

Each protonated state of the M2 channel was embedded in a pre-equilibrated water/lipid bilayer system consisting of 73 molecules of 1-palmitoyl-2-oleoyl-sn-glycerol-3-phosphatidylcholine (POPC) and 2,441 molecules of FLEXSPC water[77-79]. Sodium counterions were added by replacing a single water molecule at the positions corresponding to the lowest Coulombic energy of the ion. A total number of atoms of the whole system is approximately 12060 atoms (depending on the number of H^+ and the counterions to be added). Each system was subjected to energy minimization to remove bad van der Waals contacts and followed by an MD equilibration stage of 250 ps, during which backbone atoms of protein were restrained to their initial positions. Production runs consisted of a further 8 ns of unrestrained MD. The structural coordinates from simulations were collected every 0.5 ps for analysis.

3.2.4 NPT MD simulation of the M2 channel in POPC bilayer

MD simulations were carried out using periodic boundary and NPT conditions. A constant pressure of 1 bar was applied independently in all three directions, using a coupling constant of $\tau_p = 1.0$ ps, allowing the bilayer/protein area to adjust the optimum value. Water, lipid, and peptide were coupled separately to a temperature bath at 310 K, using coupling constant $\tau_t = 0.1$ ps[74, 80]. Long range interactions were dealt with a twin-range cutoff 1.2 nm for electrostatic interactions. The time step was 2 fs with LINCS algorithm to constraint bond length.

3.2.5 Computational Details

MD simulations were carried out using GROMACS 3.2.1[71]. The initial structure from NMR method was used, therefore, the side chain structure was improved by SCWRL3.0[81]. Structure was examined using VMD[82], RASMOL[83], and WebLab Viewer PRO 4.0. The energy minimization was setup by specifying steepest descents to remove bad van der Waals contacts. After that the position-restrained molecular dynamics was used to apply for soaking the solvent molecule into the M2 channel. A total of 8 ns MD simulations per system were simulated. The trajectories after equilibration were used to analyze the structural, dynamic and solvation properties of M2 protein.

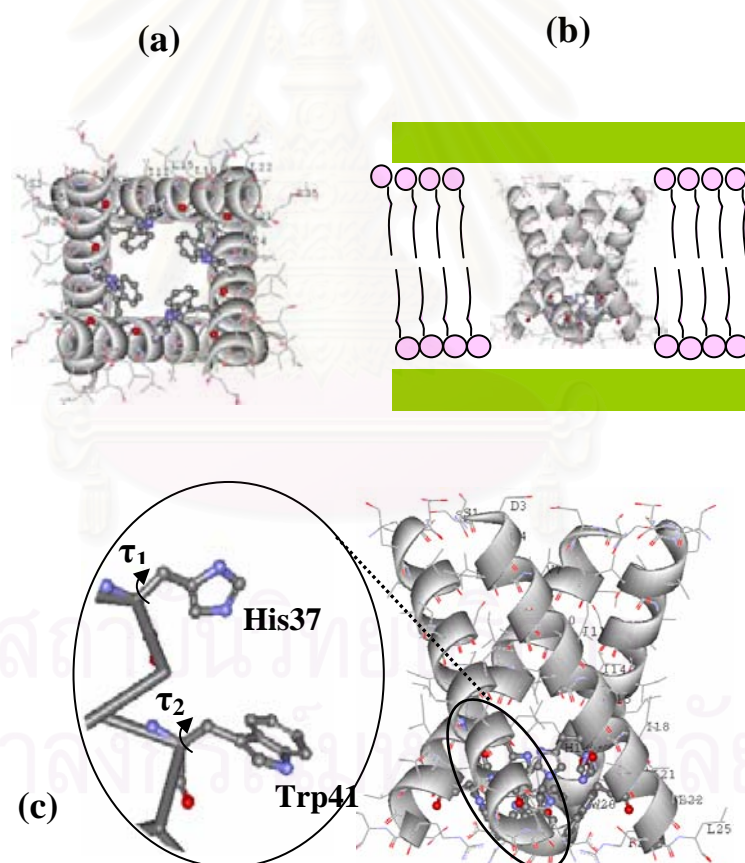


Figure 3.4 (a) top view of schematic representation of the TM-M2, (b) side view of whole system of M2 embedded in equilibrated lipid bilayer (POPC) (c) side view where the His37 and Trp41 residues were zoomed.

3.3 Results and Discussion

3.3.1 Structural Stability of M2-Channel

The structural stability of the homotetramer can be monitored by the root mean square displacements (RMSD) as a function of time. The RMSD of the backbone protein of six protonation states were calculated for 8 ns with respect to the initial configuration and plotted in Figure 3.4. The plots increase exponentially in the first ns and reach equilibrium at about 4 ns. Minimal change was observed for the 0H with the RMSD of about 2 Å. This can be due to a weak repulsion among the four non-protonated filter residues. In addition, changes of the backbone structure, compare to the initial one are in the following order: 0H < 4H < 1H < 2Ha < 3H < 2Hd. A clear description on this order as well as and the maximal change of the 2Hd system are not yet understood.

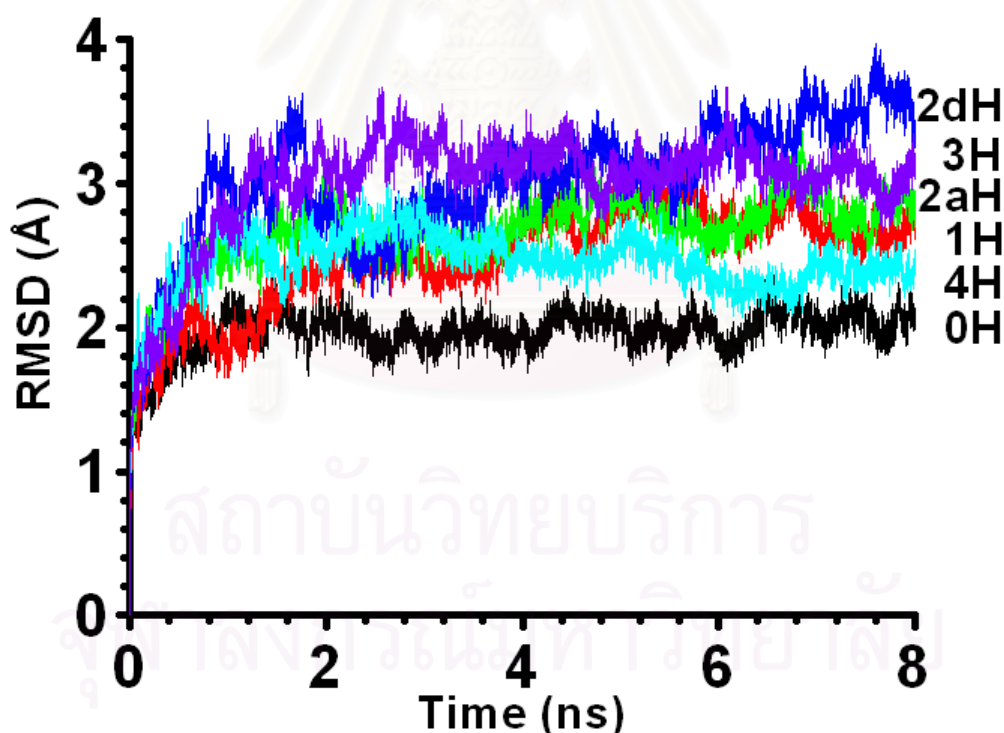


Figure 3.5 Average RMSD of entire backbone protein compare to the initial structure in the six simulated states (0H-black, 1H-red, 2Ha-green, 2Hd-blue, 3H-purple, and 4H-cyan) versus the simulation time.

3.3.2 Structural Properties of M2-Channel: Pore size

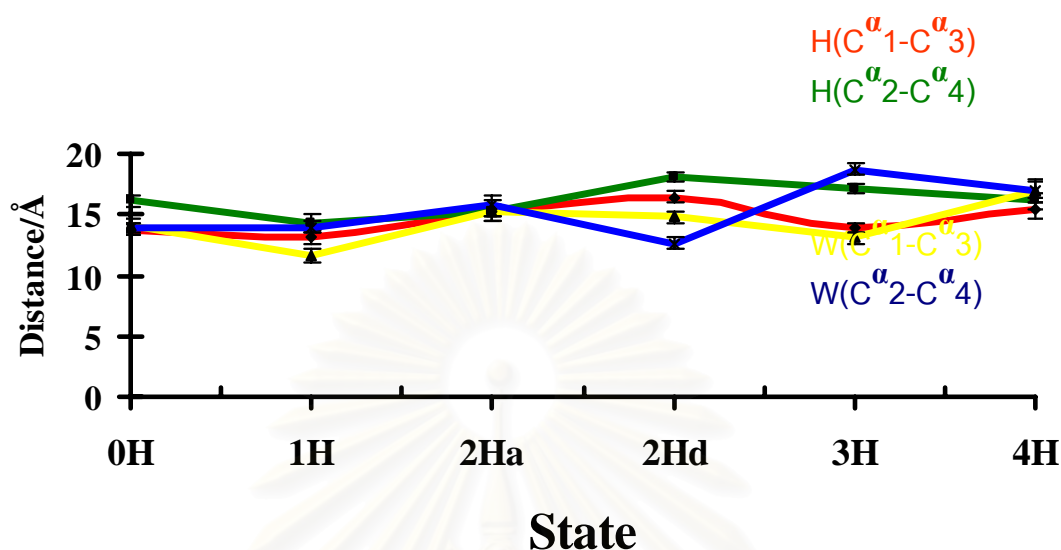


Figure 3.6 Distances between the diagonal His37 (H) and Trp41 (W) residues, measured from C^α of the *i*th and *j*th subunits, RC^α-His37_{*i-j*} and RC^α-Trp41_{*i-j*} (see also Figure 3.4c) extracted from the MD trajectories of the six simulated systems (0H, 1H, 2Ha, 2Hd, 3H and 4H).

To understand changes of the pore size of the M2 channel for the six protonation states, the distances between C^α of the opposite His37 and Trp41 residues were monitored. Evaluations were focused to both rigid and flexible parts of the four peptide subunits, represented by the C^α at the backbone and N^ε of the His37 and the terminal heavy atom of Trp41 (C^h) residues.

3.3.2.1 Distances between the backbone of the diagonal subunit: the rigid part

C^α of the His37 and Trp41 residues (see Figure 3.4c) was chosen to represent the rigid part of the M2 channel. Distances between the diagonal C^α of the *i*th and *j*th subunits, C^α of His37_{*i-j*} and C^h of Trp41_{*i-j*}, were calculated for each protonated state in terms of their distributions, changes of the distance versus probability of finding. The most probable distance for each protonation state, maximum of the distribution plot, for each plot was considered to be the optimal distance representing the backbone of the pore size and chosen to plot in Figure 3.6.

As expected, backbone of six peptide subunits is rather rigid. The plots show narrow distribution, in changing from one to the other protonation states. In comparison between pore sizes represent by the His37 and Trp41 residues, significant difference was detected for the 2Hd system in which that of the His37 is slightly larger than that of Trp41.

3.3.2.2 Distances between terminal side-chain of diagonal subunit: the flexible part

Beside the distribution of the distances between the diagonal C^α of the His37 and diagonal C^h of the Trp41 which was supposed to represent the rigid part of the M2 pore size (Figure 3.6), the smallest part of the pore size of the channel was assumed to determine by flexibility and movement of the N^ϵ of the His37 and C^h of the Trp41 of the diagonal subunits (see Figure 3.4c). Notations $R N^\epsilon$ -His37_{i-j} and RCH -Trp41_{i-j} were, then, used for simplicity. Calculations were carried out in the same manner as that of the C^α (Figure 3.6). As a function of the protonation states, the results were plotted in Figure 3.7.

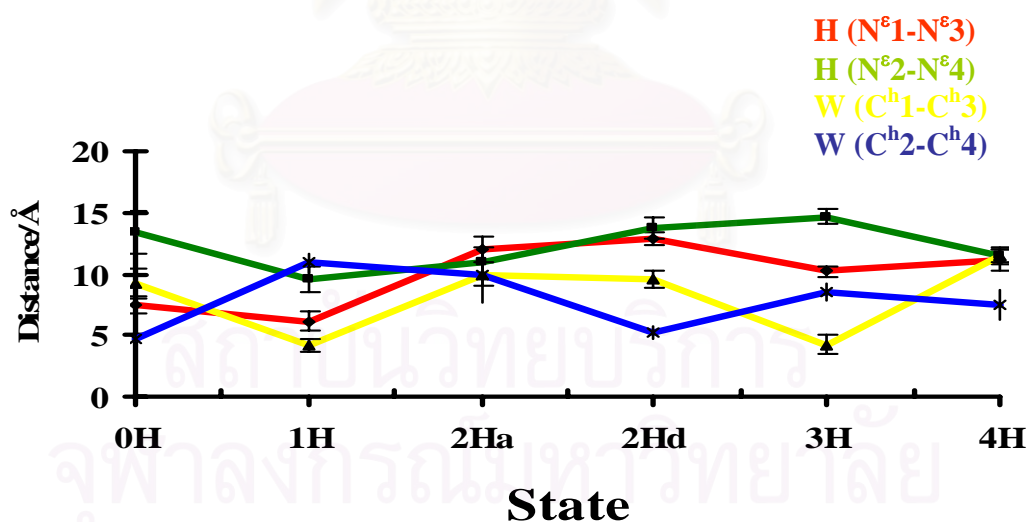


Figure 3.7 Distances between the diagonal i^{th} and j^{th} subunits measured from the N-epsilon (N^ϵ) of His37 (H) and C (C^h) of Trp41 (W), $R N^\epsilon$ -His37_{i-j} and RCH -Trp41_{i-j} (see also Figure 3.4c) for the six simulated systems (0H, 1H, 2Ha, 2Hd, 3H and 4H).

Flexibility of the end of the side chains of both His37 and Trp41 residues were clearly exhibited, especially at the 0H, 1H, 2Hd and 3H protonated states. Due to complexity and flexibility of such side chains, a clear relation, as a function of protonation state, cannot be made.

3.3.3 Characteristic of the Gating

Beside the inter-subunit distances, characteristics of the pore size can be governed by orientation of the His37 and Trp41 side chains. Here, torsional angles of both His37 and Trp41 were investigated along the simulation time. The size of pore not only depends on the distances of inter-subunit but the orientation of sidechain of His37 and Trp41 residues are also effect the size of pore. So, the two types of torsion (τ_1 and τ_2 see Figure 3.4c) of both His37 and Trp41 were investigated along the simulation (see Figure 3.8) to get more information in details.

3.3.3.1 Side chains translating

The translations of side chain of His37 and Trp41 in each subunit were investigated (see Figures 3.8a and 3.8b). From the starting structure, the torsions of His37 and Trp41 are about -180° and 180° of His37 and Trp41, respectively. The results of His37 side chain moving in 2Hd, 3H, and 4H slightly move (see Figure 3.8a). For 0H, 1H, and 2Ha, the plots of torsions show that some side chain translated. While the side chain of Trp41 indicated that most of torsions move in the opposite direction.

3.3.4 Water Transportation through M2 Channel

3.3.4.1 Binding of water molecule to the selectivity filter residues

In addition to the structural properties of M2 protein in different states, the position and distribution of water molecules via moving through the M2 channel were evaluated in terms of atom-atom radial distribution function (RDF) $—g_{xy}(r)$, the probability of finding an atom of type y in the spherical volume of radius r around the central atom of type x. Here, distributions of O and H atoms of water molecules around the N^{ϵ} and N^{δ} atoms of His37 for the six protonation states (0H, 1H, 2Ha, 2Hd, 3H, and 4H) were calculated and plotted in Figure 3.9a. The running integration

numbers, corresponding to coordination number (CN), were also given in the same plot. Based on the atomic topology and its environment, the RDFs are classified into 4 groups centered at the (A) non-protonated N^δ , (B) N^ϵ at the same subunit as A, (C) protonated N^δ and (D) N^ϵ at the same subunit as C. Beside the RDFs shown in Figure 3.9a, schematic representations of the A-D regions are accordingly given as Figure 3.9b. Integration number up to the first minimum of each RDF, denoted number of water molecule localized at each region, was given in parenthesis.

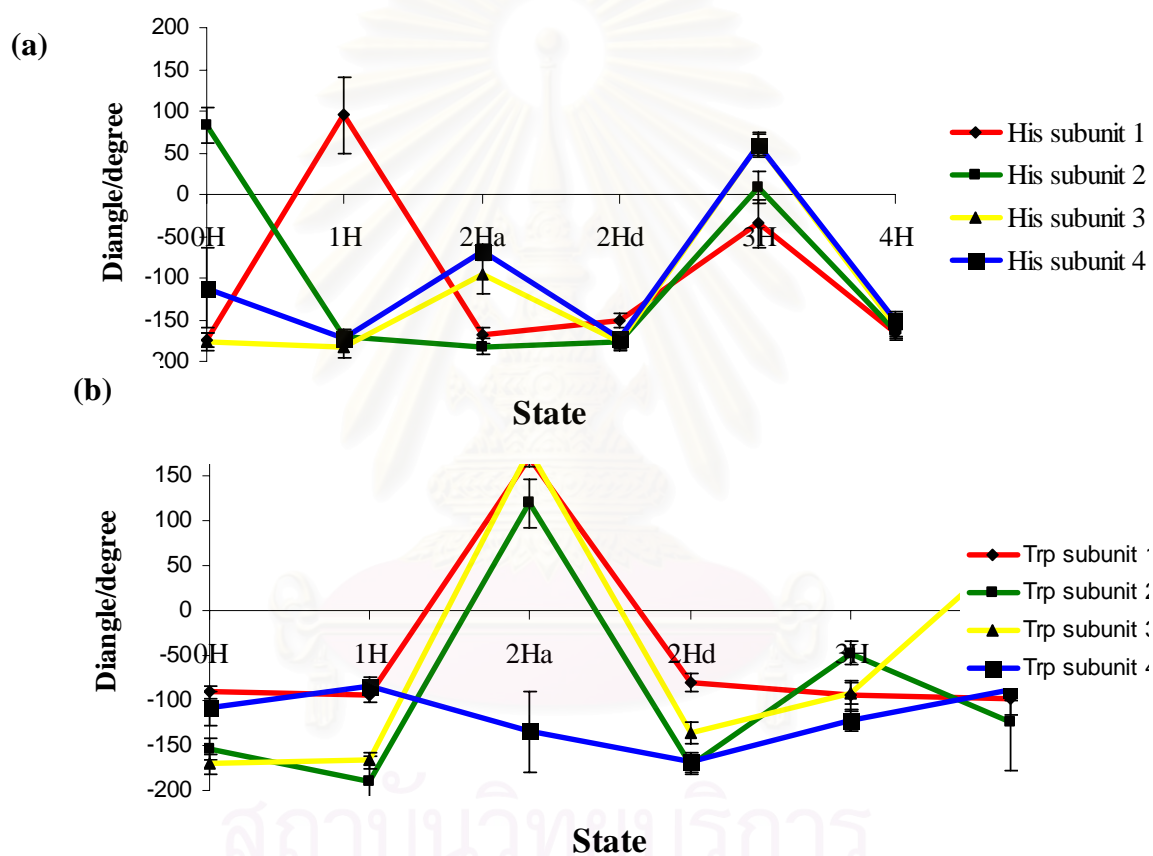


Figure 3.8 The average torsion angles of the four subunits of the His37 (a) and Trp41 (b) side chains.

The RDFs of type A centered at non-protonated N^δ to H and O atoms of water for the 0H, 1H, 2Ha, and 2Hd states (labeled as A and respectively shown in the left top of Figure 3.9a) demonstrate the first peak at 1.95 Å and 2.95 Å, respectively. Sharpness as well as their pronounce characters indicate strong hydrogen bond

between the non-protonated N^δ and water molecules. The difference between the distances to the two maxima of ~ 1 Å reveals the linear hydrogen bond where water molecule points one H atom to the N^δ of His37. Integration number up to the first minima of the RDFs yields 0.1, 0.5, 0.1 and 1.0 water molecule for the 0H, 1H, 2Ha, and 2Hd protonation states, respectively. These numbers demonstrate average number of water molecule which coordinated at the region A (see regions A for the 0H, 1H, 2Ha, 2Hd, and 3H protonation states in Figure 3.9b). Interestingly, the 2Ha state ($CN = 1.0$) is better solvated than the 2Hd one ($CN = 0.1$), *i.e.*, diprotonation at the diagonal subunit (2Hd) leads to higher hydrophilicity of the M2 channel than that at the adjacent position 2Ha. This can be due to the symmetry of protonation. And there is no water in this region in the 3H.

Consider the RDFs centered at N^ϵ lying at the same subunit as the non-protonated N^δ (see also labeled B for the 0H, 1H, 2Ha, 2Hd and 3H systems, shown in Figure 3.9), no water molecule can approach to this atom of the non-protonated state, 0H and 3H. It is interesting to note that the 1H and 2Hd states are equivalently solvated. As can be seen from Figure 3.9, their RDFs to O and H atoms of water show first pronounced peak at 2.95 Å and 3.80 Å, respectively, with the $CN = 0.5$ water molecule. These events tell us that during the simulation time, (i) regions B of the 1H and 2Hd systems are 50% ($CN = 0.5$) occupied by water molecule. (ii) This water forms hydrogen bond with N^ϵ (O...O distance = 2.95 Å) and points O atom to the N^ϵ (distance to the first peak of the RDF to O atom appears at shorter distance than that to H atom of water). (iii) Broaden of the RDF first peak to the H atom indicates rather free orientation of water molecule, and (iv) Non-zero of the RDF first peak denotes solvent exchange from and to region B (with 50% occupation). In contrast to the conclusions for the 1H and 2Hd states, diprotonated state at the adjacent position, 2Ha, causes much lower hydrophobicity of the N^ϵ atom, with 5% occupation ($CN = 0.05$).

No difference was found between the solvation, at the same protonation state, of the protonated N^δ (RDF-plot in regions C in Figure 3.9) and the N^ϵ atom lying at the same subunit (plots and regions D in Figure 3.9). All RDF to O atom of water in regions C and D shown very sharp and pronounce first peak centered at 2.95 Å indicating a strong hydrogen bond between water and both N^δ and N^ϵ atoms. An appear of the pronounced second peak at 4.20 Å is due to both solvations, *i.e.*, water

molecule located under the first peak at 2.95 Å of the N^ϵ -O RDF is, at the same time, counted to appear at 4.95 Å of the N^δ -O RDF, and vice versa. In another word, if $R_{N^\epsilon-O1} = R_{N^\delta-O2} = 2.95$ Å, then, $R_{N^\epsilon-O2} = R_{N^\delta-O1} = 4.95$ Å where O1 and O2 are oxygen atoms of water molecules 1 and 2 which form linear hydrogen to N^ϵ and N^δ , respectively. In terms of coordination number, integration up to the first minima of all RDFs leads to the CN of 1.0 water molecules. These numbers were, then, summarized in regions C and D of Figure 3.9b.

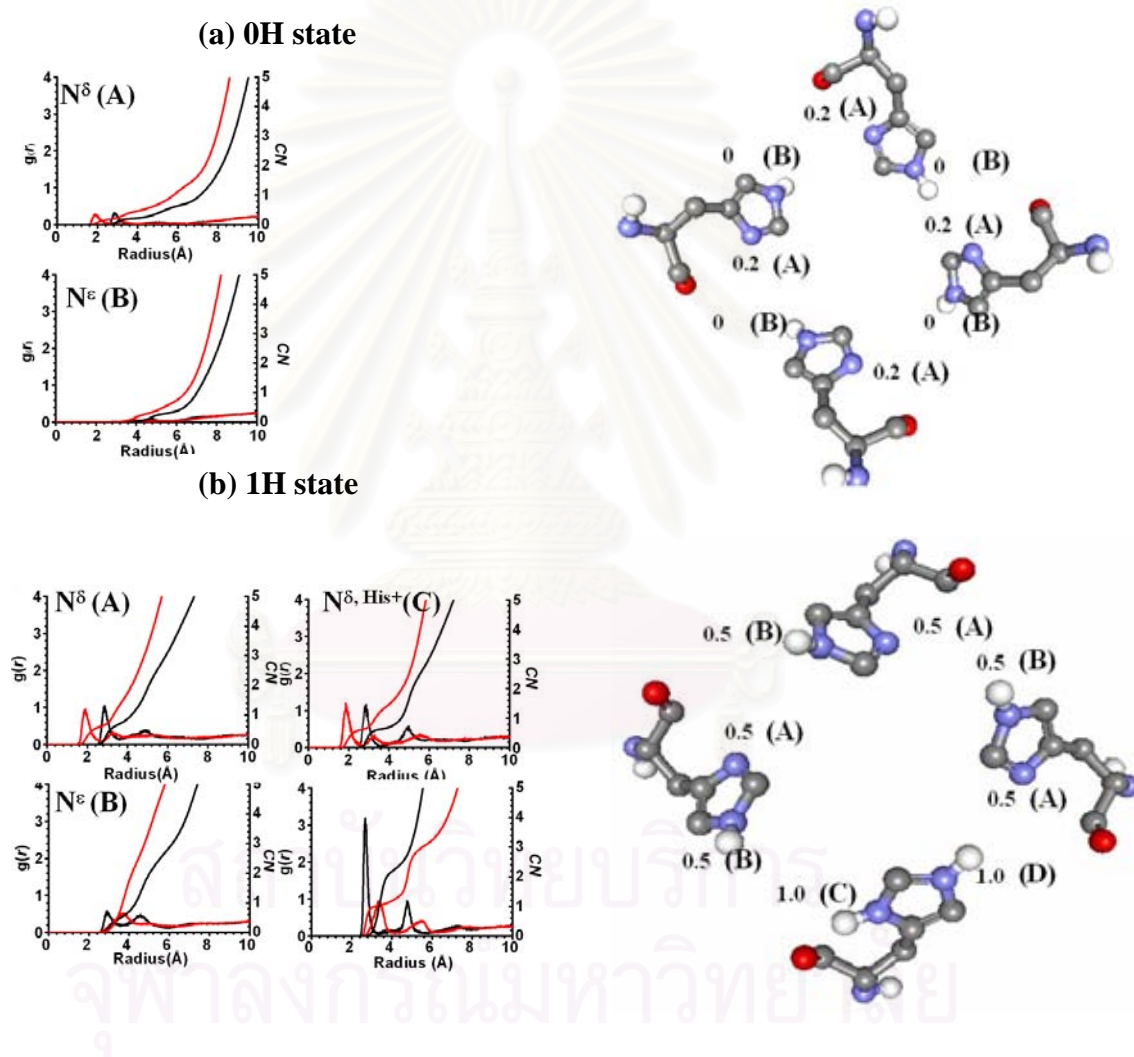
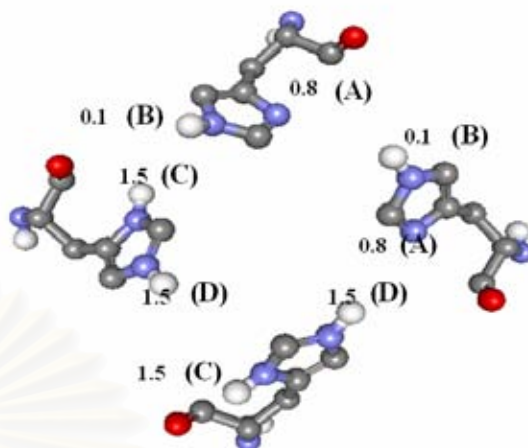
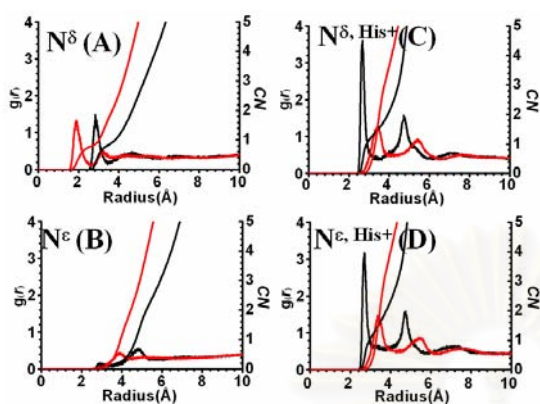
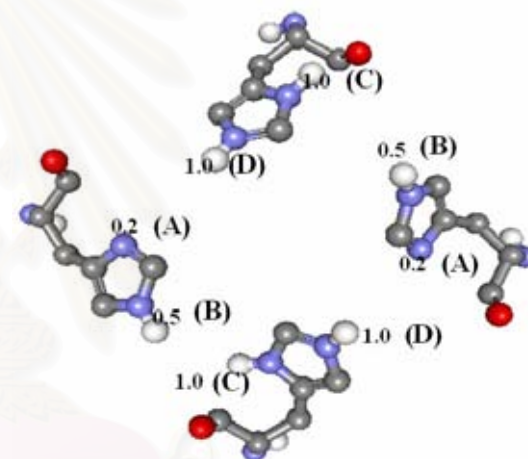
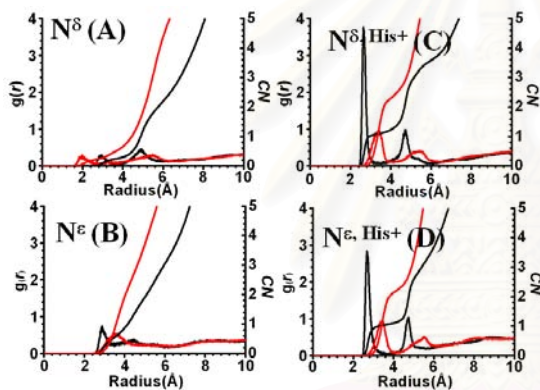


Figure 3.9 RDF average of six systems 0H, 1H, 2Ha, 2Hd, 3H, and 4H, respectively. (A) and (B) average RDF at region of nonprotonated- N^δ and N^ϵ at the same subunit, (C) and (D) average RDF at region of protonated- N^δ and N^ϵ at the same subunit. Schematic representations of His37 tetrad where the numbers are water in each region are shown in the right of RDF.

(c) 2Ha state



(d) 2Hd state



(e) 3H state

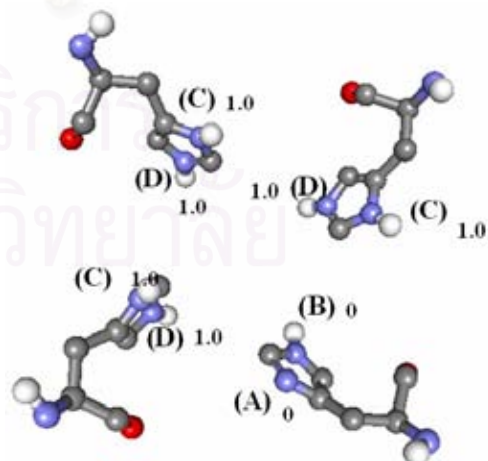
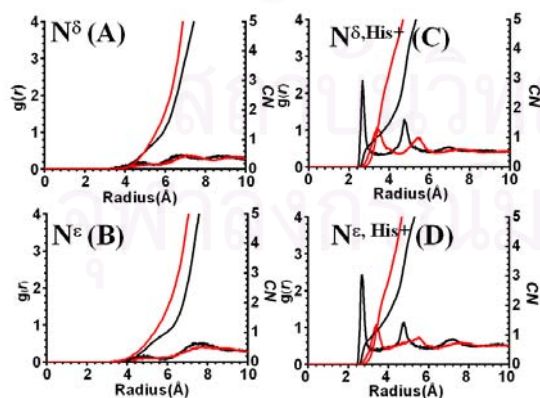


Figure 3.9 (continue)

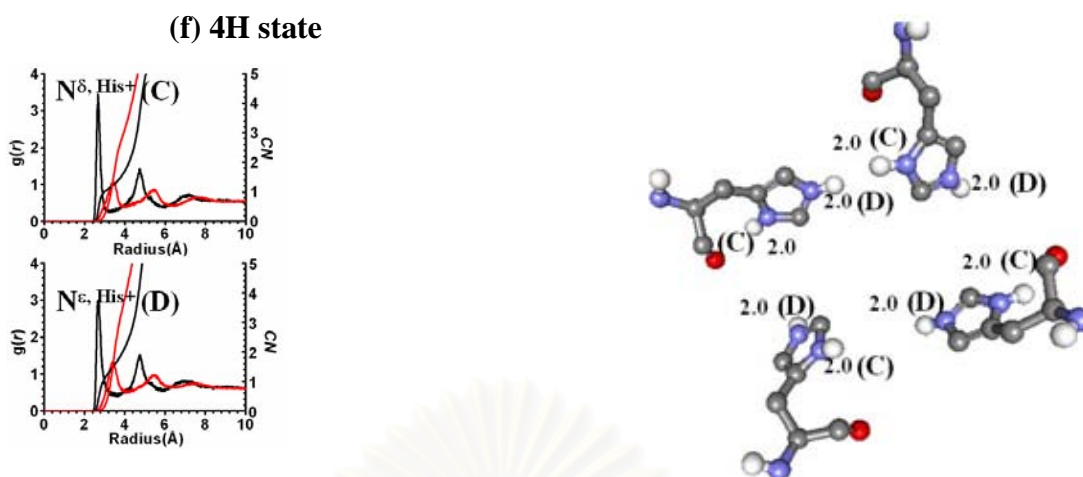


Figure 3.9 (continue)

3.3.4.2 Atomic Density Profile

Density profiles of each component (M2, POPC, and SOL) were evaluated to investigate the content of water in the protein pore. The density plots of water were zoomed in the all systems to quantitatively measure water in the channel. It can be clearly seen from the insets that water molecule cannot move through the M2 channel in the 0H and 2Hd protonated states. Water transportation can be taken place for the 2Ha and 4H states. Interestingly, the 1H pore was fully filled by water up to the His37 residue (the inset of plot (b) appears zero at 40 Å) but water cannot move through this filter residues.

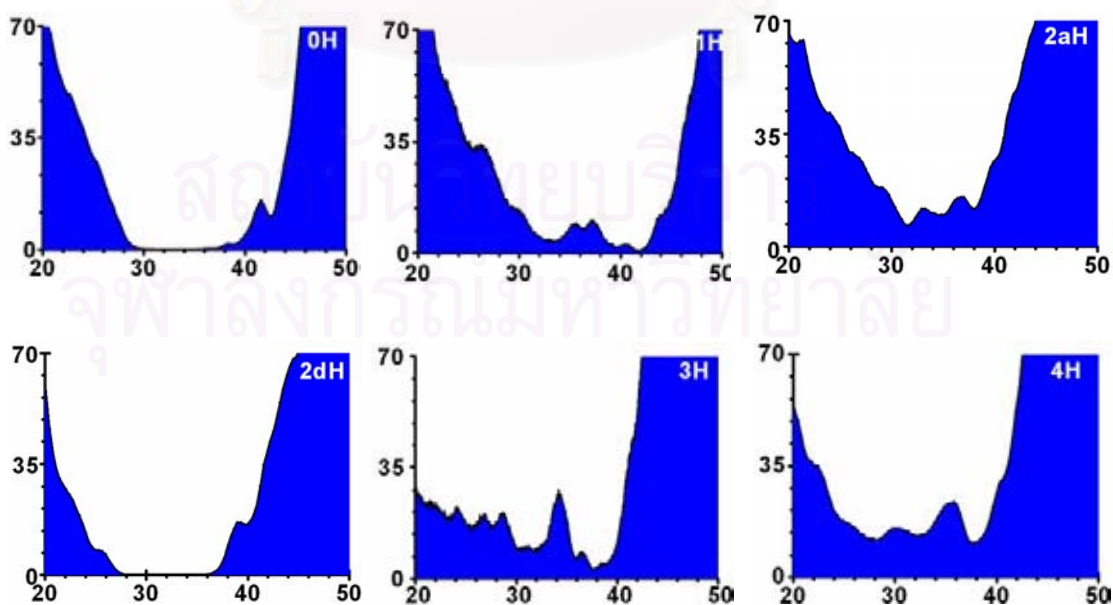


Figure 3.10 Water Densities of all states were plotted along M2 channel (Å).

In the nonprotonated state, water molecule in the pore is occluded from the constrictive region of the channel (Figure 3.10a). There is no water molecule crossing from one side of the lipid bilayer to the other side during the course of MD simulation. This indicated the channel does not permeate any water molecule and therefore it corresponds to the closed state channel (Figures 3.10a and 3.10b). On the other hand, the permeation of water to across membrane bilayer is found for diprotonated, triprotonated and tetraprotonated systems (Figures 3.10c-3.10f). However, the flow of water is not continuous for diprotonated state of the channel (Figures 3.10c and 3.10d). This might indicated that the channel is partially open. In triprotonated and tetraprotonated systems (Figures 3.10e and Figure. 3.10f), the movement of water crossing the bilayer was constantly observed. The results suggested that the channel is fully activated and it corresponds to the open state conformation of the channel.

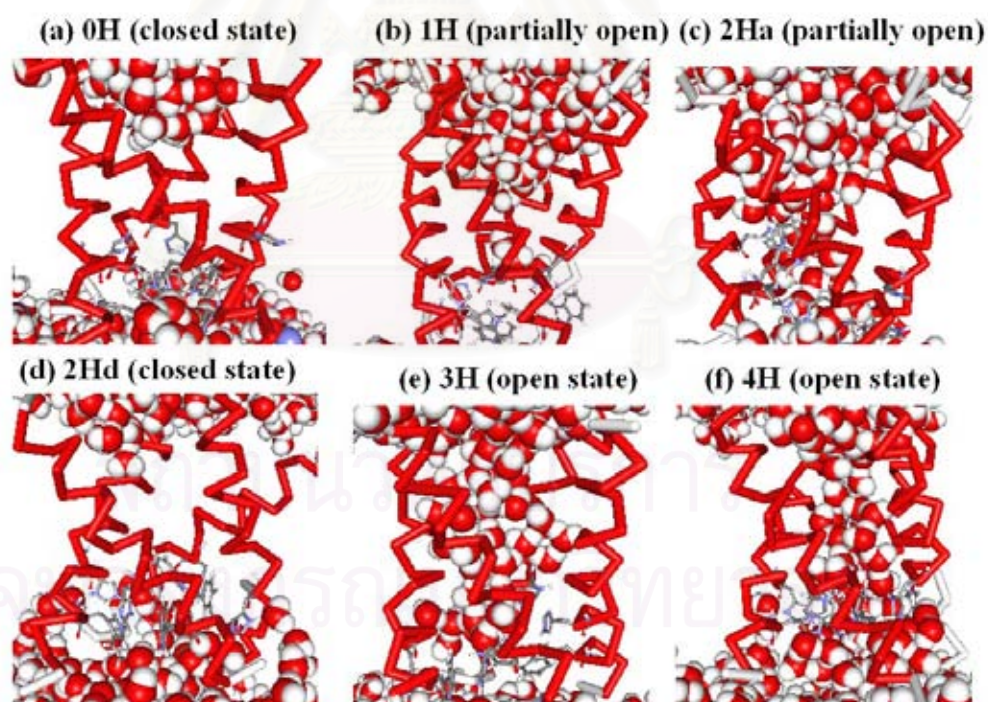


Figure 3.11 Snapshots of six states were represented with space-filled of water molecules.

3.4 Conclusion

MD simulations were carried out for 8 ns at different protonation states, the selectivity filter residue of M2 channel. The results shown that water molecule cannot move through the constrictive region of the channel in non-protonated state. This corresponds to the closed state of the M2 channel. The channel is partially open for the 1H-, 2Ha-, 2Hd-M2 states and fully open for 4H-M2 PS system.



สถาบันวิทยบริการ
จุฬาลงกรณ์มหาวิทยาลัย

CHAPTER 4

MD SIMULATIONS OF WILD-TYPE M2 CHANNEL- INHIBITOR COMPLEXES

4.1 Introduction

Amantadine and its adamantane's derivative are specific anti-influenza drugs. They inhibit viral replication, primarily by blocking proton transport through the proton-selective M2 channel. Without the acidification of the viral interior, the uncoating process cannot be occurred. In this chapter, molecular dynamics simulations of wilde-type M2 channel complexed with the two inhibitors were carried out in a fully hydrated lipid bilayer. The simulations of six possible protonation states of His37 (0H, 1H, 2Ha, 2Hd, 3H and 4H) were investigated in the presence of the drugs in order to understand the mechanism of inhibition.

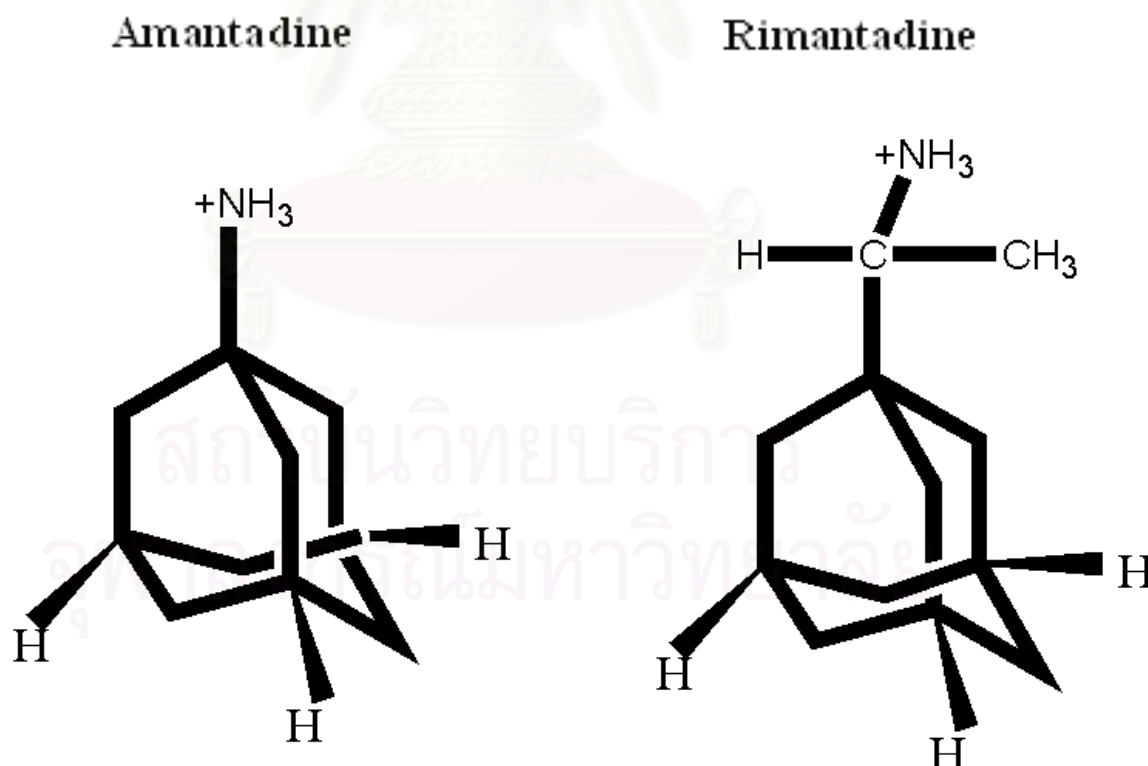


Figure 4.1 Adamantane derivatives of M2 inhibitors

4.2 Methods

4.2.1 Construct an initial model

The model of the M2 channel was taken from Protein Data Bank (2H95)[69]. Assembly of the helical bundles of the M2 channel was based on the 3D structure predicted by NMR measurement. Six MD simulations were carried out on the basis of the ionizable histidine at N^c. These are non- (0H), mono- (1H), di- at adjacent position (2Ha), di- at diagonal position (2Hd), tri- (3H) and tetra-protonation state (4H). Structures of amantadine and rimantadine were built and optimized using Gaussain03, HF/6-31G*. The two inhibitors were docked into the pore of M2 channel using Autodock 3.0 program and manual modeling[84].

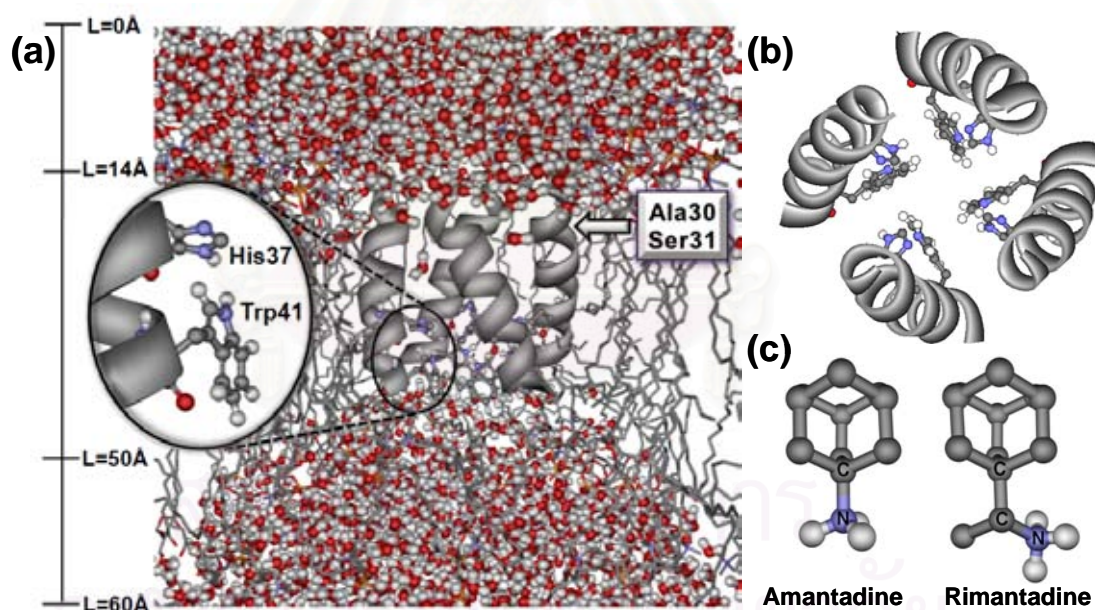


Figure 4.2 Schematic of M2 channel and its inhibitors (A) Side view of the M2 channel with Ala30, Ser31, His37 and Trp41 residues, (B) top view of the M2 protein channel, and (C) the two inhibitors, where the distance scale L was used for the density plot shown in Figure 2. $L = 14 \text{ \AA}$ and $L = 50 \text{ \AA}$ denote coordinates of the ends of the N- and C-terminals, respectively.

4.2.2 Setup of membrane/protein systems

The influenza A/M2 bundle was embedded into preequilibrated lipid bilayer, initially made up of 128 molecules of 1-palmitoyl-2-oleoyl-sn-glycerol-3-phosphatidylcholine (POPC) lipid embedded in 2460 molecule of FLEXSPC water[77, 78]. The GROMACS package is used to set up the simulation system of bundle of M2 complex into equilibrated lipid bilayer[71, 85]. Na⁺ counterions were added to neutralize the system charge according to the protonation state of the channel by replacing water molecules at the positions corresponding to the lowest Coulombic energy of the ions.

The protein-bilayer-water systems were energy minimized, followed by equilibration in two stages. Firstly, the system underwent 0.5 ns of an MD run with positional restraints on the protein. In all other molecules, all bond lengths and angles were constrained. Secondly, the system underwent 0.5 ns of an MD run with positional restraints on the protein atoms, so as to improve the packing of lipids around the protein. Thereafter, the equilibrated systems were subjected to 8.0 ns MD simulation.

4.2.3 MD Simulation details

The simulations were carried out using GROMACS 3.2.1 package with the GROMOS87 forcefield[71]. All simulations were conducted by the LINCS algorithm[74] to constrain bond lengths and angle of hydrogen atoms, using time step of 2 fs. Systems were coupled separately to a Berendsen temperature bath at 310 K, using coupling constant τ_T 0.1 ps[86]. The constant pressure of 1 bar was kept constant by semiisotropic coupling of the system to a Berendsen pressure bath[86]. Long-range interactions were involved with a twin-range cutoff: 1.2 nm for a van der Waals interactions, and 1.2 nm for electrostatic interactions computed using PME algorithm.

4.3 Results and Discussion

4.3.1 Blocking of water transport

Water transport was monitored in terms of water density across the M2 channel where $L = 14 \text{ \AA}$ starts from the N-terminal (see Figure 4.2). To understand the movement of the inhibitors and their locations relative to the histidine gate and pore lining Ala30, distributions of inhibitors as well as the average coordination of the protonated and non-protonated His37 and four Ala30 were also plotted in Figure 4.3.

Without the inhibitor, water density for the 0H state (Figure 4.2, top panel, dashed line) decreases exponentially and approached zero at $\sim 28 \text{ \AA}$, then starting to increase at $\sim 40 \text{ \AA}$. This character, which is also true for 2Hd state, indicates a solvent free-region where water cannot penetrate through the channel. In conclusion, among the six states of M2 in free form, water transport was observed to take place in the 1H, 2Ha and 4H states. A discrepancy was found in comparison with the previous MD results for free M2 channels[55], in which water was also detected to move through the channel in the 2Hd state. For clarification, consider the fact that water transport can take place in the M2 channel only at $\text{pH} < 7$ [26, 35, 61, 87], for high protonation states of the histidine gate. It was recently found using NMR measurements that the 2Hd states yield a pH of 7.3[31]. This datum supports our finding clearly.

For the M2-inhibitor complexes, non-zero water densities were noticeably found only in the 2Ha and 4H states of the amantadine complexes and, slightly, in the 2Hd state of the rimantadine system. This leads to the clear conclusion that water was better inhibited by rimantadine than amantadine. This fact was strongly supported by the experimental evidence in which the IC_{50} value of $0.98 \pm 0.10 \text{ \mu g}\cdot\text{ml}^{-1}$ for M2-rimantadine is over 10-fold lower than that of $13.8 \pm 1.7 \text{ \mu g}\cdot\text{ml}^{-1}$ for the M2-amantadine complexes.

In terms of inhibitor mobility in the M2 channel, it was shown by the distribution plot of the inhibitors (filled areas in Figure 4.2) to be localized at specific binding sites of the M2 channel. It can be also seen from the plots that distance from the pore (N-terminal) of the channel to the inhibitor's center of mass (D_{dept}) depends directly on the protonation state of the protein, *i.e.*, the inhibitors were located deeper in the channels of lower protonation states. This fact can be described by an increase of the repulsive interaction due to an increase of positive charge on the histidine gates

of the higher protonation states. However, no relation can be inferred regarding the D_{dept} values of the two inhibitors. Amantadine can approach closer to the histidine gate for the 0H and 2Hd states, while rimantadine is closer for the 1H and 2Ha states (the average position of histidines is shown by vertical dashed lines in Figure 4.2). Excluding the 4H system, where the inhibitors were found to be located almost above the opening pore, interest is focused on the 2Ha and 2Hd states, in which non-zero water densities were found beyond the distribution of the inhibitor's coordinates. In other words, water was observed to penetrate through the inhibitors. An answer to this fact relates directly to the inhibitor-solvent and inhibitor-protein interactions, which are described in the next sections.



สถาบันวิทยบริการ
จุฬาลงกรณ์มหาวิทยาลัย

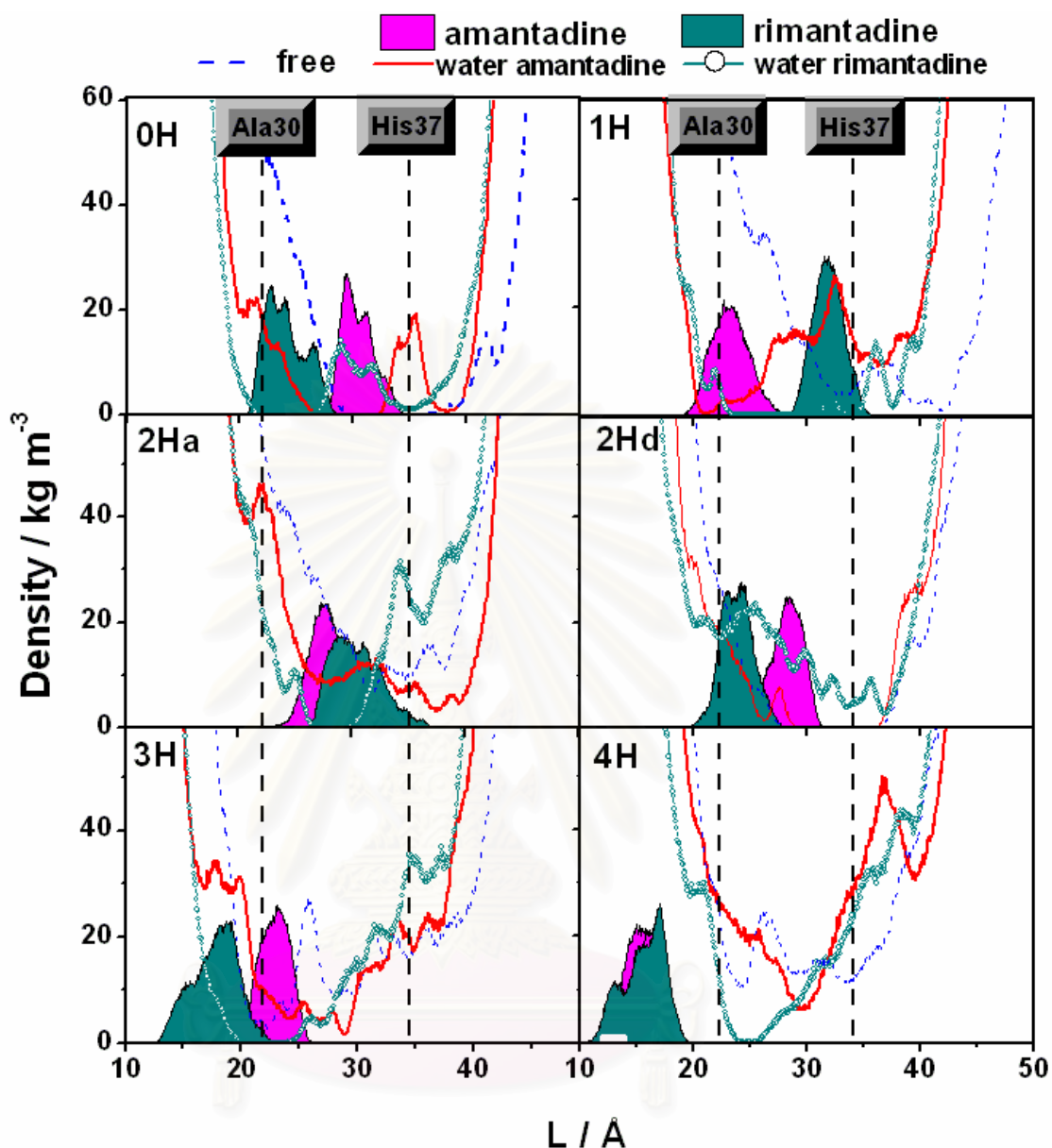


Figure 4.3 Water density along the M2 channel (see Figure 4.2 for the definition of the distance L) for free M2 and its complexes with amantadine and rimantadine in the 6 protonation states (0H, 1H, 2Ha, 2Hd, 3H and 4H), where the filled areas (magenta for amantadine and dark cyan for rimantadine) represent distributions of the inhibitor's coordinates along the channel and the vertical dashed lines indicate average positions of the four Ala30 and four His37.

4.3.2 Inhibitor-solvent interaction

The inhibitor-solvent interaction was monitored in terms of atom-atom radial distribution functions (RDFs), expressed as $g_{ij}(r)$, the probability of finding a particle of type j in a sphere of radius, r , around a particle of type i . Figure 4.3 shows RDFs centered on the N atoms of inhibitor side chains and the O atoms of water. The corresponding first-shell coordination numbers integrated up to the first minimum are also indicated. All plots show a first sharp peak at $\sim 3 \text{ \AA}$, indicating that side chains of both inhibitors were firmly solvated. No significant difference was found in terms of the peak position. A clear conclusion can be drawn regarding the first shell coordination numbers. Excluding the 4H state, the number of water molecules around the amantadine side chain is significantly higher than for rimantadine, *i.e.*, the RDF data provide clear evidence that amantadine is solvated by more water molecules than rimantadine.

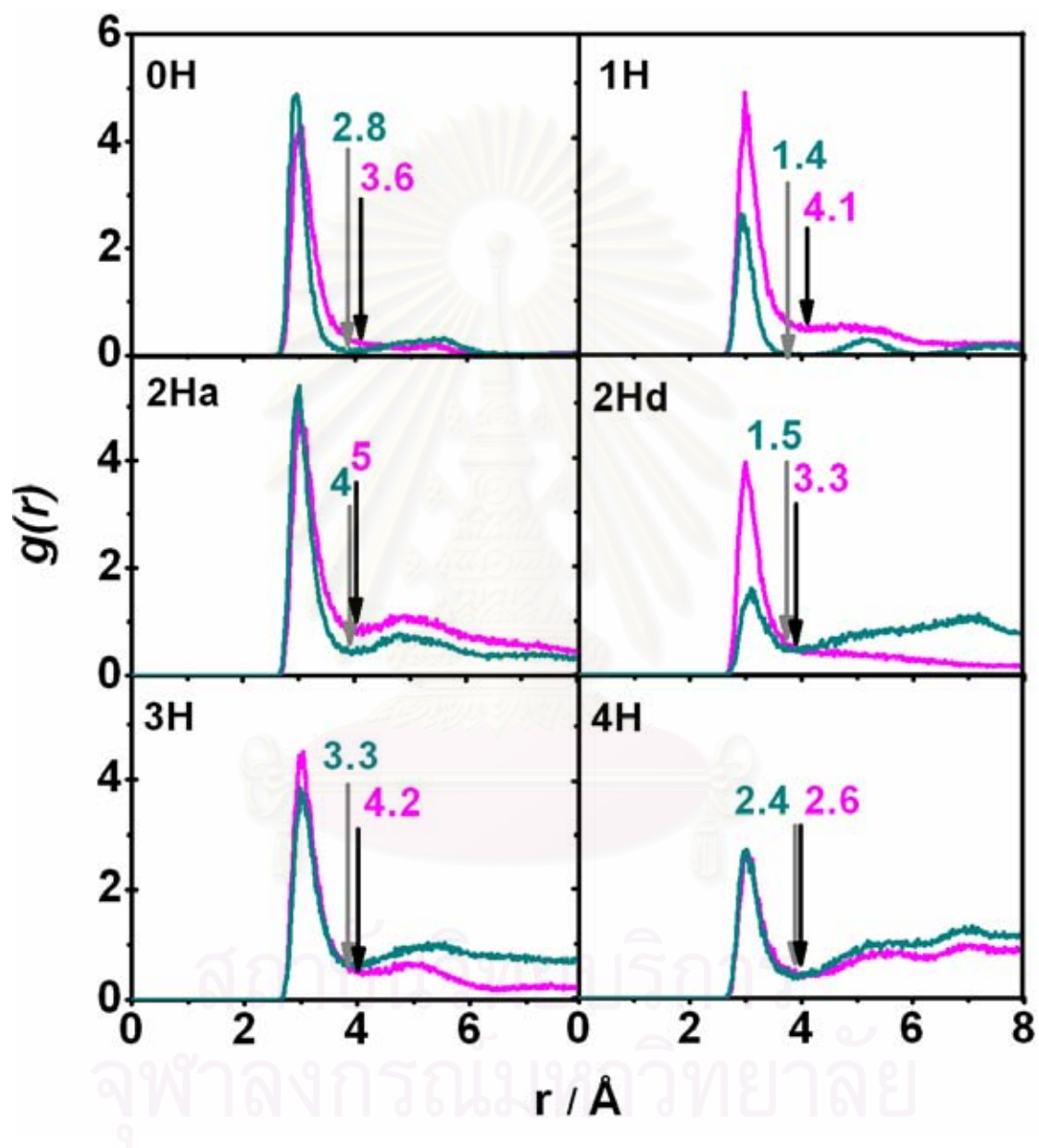


Figure 4.4 Radial distribution functions, $g(r)$. Plots of $g(r)$ from nitrogen atoms of amantadine (magenta) and rimantadine (dark cyan) to oxygen atoms of water. First-shell coordination numbers integrated up to the first minimum (marked by an arrow) are indicated.

4.3.3 Mobility of the inhibitor in the M2 channel

In addition to determining the depth to which inhibitors can penetrate into the channel (section 4.2.1 and filled areas shown in Figure 4.3), we also determine their locations in the lateral x and y dimensions. In Figure 4.3, the center of mass of the adamantane group (excluding the side chains) is projected onto the square formed by the four C_{α} atoms of the histidine tetrad, leading to the following conclusions: (i) All peaks are sharp and pronounced, located away from the center of the xy -plane. This indicates localization of the inhibitors close to the residues of M2. This finding agrees well with the inhibitor-protein interaction data described in section 4.2.4 (ii) The plots for rimantadine are slightly broader than those for amantadine. This confirms the N-O RDFs shown in Figure 4.4, where amantadine side chain was found to bind more strongly to the solvated water molecules compared with rimantadine, thus allowing the solvated rimantadine to move more freely without carrying any nearest-neighbor water molecules.

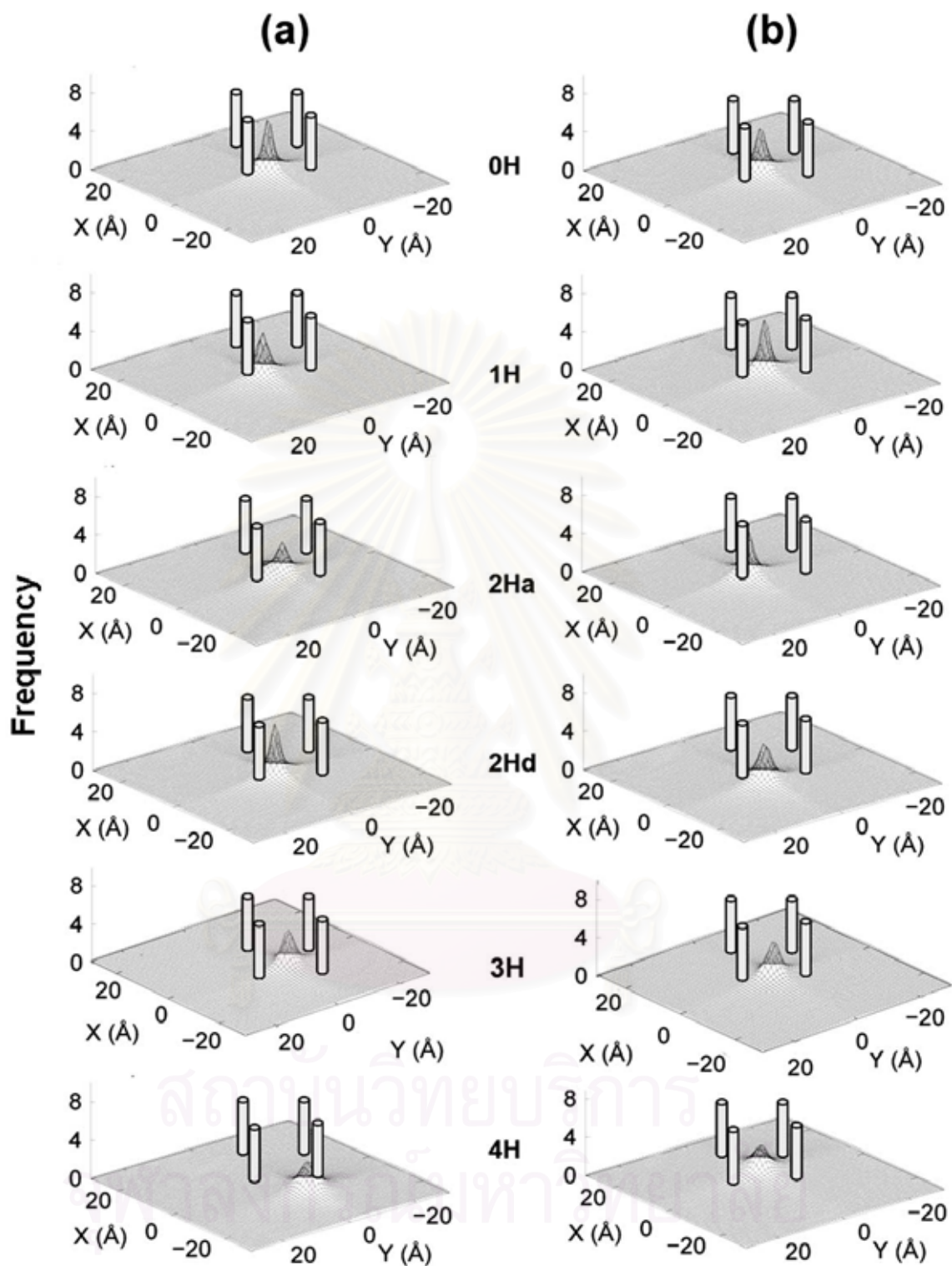


Figure 4.5 Density of M2 inhibitor center of mass. Frequency (vertical axis) of center of mass locations from the ten simulated systems of (A) amantadine and (B) rimantadine projected onto the square (xy-plane) formed by the four C_{α} atoms (represented by cylindrical tubes) of the histidine tetrad.

4.3.4 Inhibitor binding site in the M2 channel

The number and percentage of hydrogen bonds between inhibitor molecules and the protein were investigated separately for the 4 units of the M2 tetramer. The bonds are defined by the default of the GROMACS program, *i.e.*, proton donor-acceptor distance ≤ 3.5 Å and donor-H-acceptor bond angle $\geq 120^\circ$. The results are shown in Figure 4.5.

Again, the 4H state was not taken into consideration. As shown in Figure 4.5, the plots lead to the following conclusions: (i) The inhibitors were found to form hydrogen bonds with only three binding sites, located at the opening pore residues (Ala30 and Ser31) and the histidine gate (His37). Interestingly, Ala30 and Ser31 are the two residues previously associated with resistance to amantadine[24, 61, 88, 89]. (ii) As expected, the inhibitors were observed to bind very weakly to the channel due to their allosteric hindrance. The strongest hydrogen bond is formed between the imidazole ring of His37 and the ammonium group of the inhibitor in the 0H-amantadine and 1H-rimantadine complexes, with $\sim 55\%$ occupation. (iii) More hydrogen bonds and a higher percentage occupation were formed in the less protonated complexes, 0H and 1H, than in the more protonated complexes, 2Ha and 2Hd. This is due to the effect of repulsion between the $-\text{NH}_3^+$ groups of inhibitors and the positively charged imidazole ring of histidine in the more protonated systems, which contained a larger amount of protonated His37. The observed data are directly related to the distance from the pore (N-terminal) of the channel to the inhibitor's center of mass, D_{dept} , as shown in Figure 4.3. (iv) An answer to the previously mentioned question of why water was better inhibited by rimantadine than amantadine is indicated by very weak hydrogen bonding in the 2Ha state (Figure 4.6). Rimantadine was detected to be localized slightly closer to histidine gate compared with amantadine (see distributions of the inhibitors in Figure 4.3) and can facilitate the orientation of His37 to close the channel. The influence of the inhibitors on the His37 orientation can be obviously exhibited by the protein-amantadine (0H state) and protein-rimantadine (1H state) configurations as mentioned in (ii). This finding agrees well with the mechanism proposed by Pinto et al. based on results from the cysteine scanning mutagenesis technique[20, 87] which stated that inhibitor binding to the His37 side chain can interfere with the histidine facilitation of proton

conductance. The proposed mechanism was also supported by the NMR results published recently by Hu and coworkers[37].

Besides the above mechanism, an alternative mechanism was indicated by the interaction between inhibitors and two opening pore residues, Ala30 and Ser31, which are located approximately 5 Å from the N-terminal (see also Figure 4.1a). Binding to either Ala30 or Ser31 was detected in almost all states of the drug-blocked complexes as shown in Figure 4.6. This mechanism agrees well with a hypothesis that the inhibitor acts as a blocker by interacting with the mouth of the M2 pore[59, 64]. However, referring to the lower inhibition of amantadine than rimantadine in the 2Ha state (see Figure 4.3), this inhibition mechanism could have a lower efficiency compared with that where inhibitor binds with the histidine gate. A clear picture of the two mechanisms and detailed descriptions are given again in Figure 4.8 and section 4.2.5, respectively.



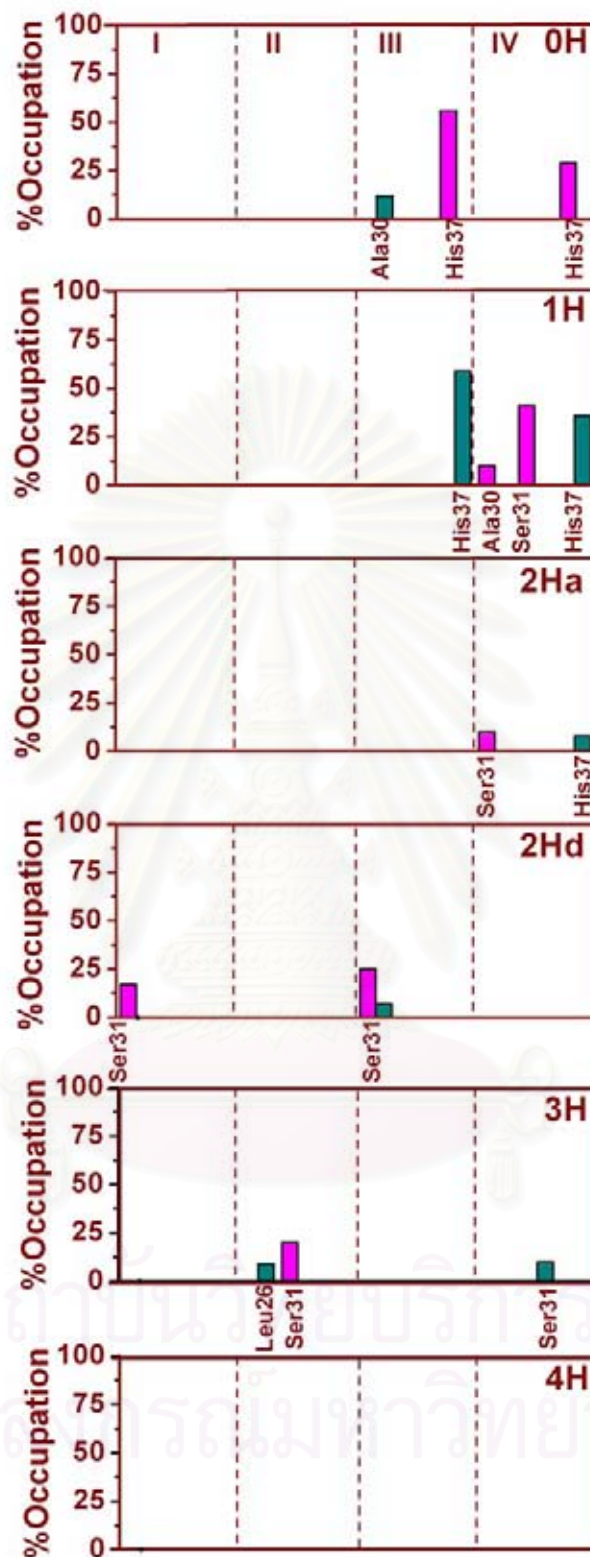


Figure 4.6 Hydrogen bond occupations between M2 residues and inhibitors

The hydrogen bond occupation between M2 residues and the inhibitors amantadine (magenta) and rimantadine (dark cyan) for the eight simulated systems, where I-IV denote the four units of the M2 protein tetrad.

4.3.5 Orientation of Inhibitor in M2 channel

The orientation of the inhibitor embedded in the channel was visualized in terms of the distribution of an angle θ (see inset of Figure 4.6). The angle was defined by two vectors, of which one points along the C-X bond, where X denotes an N atom for amantadine and a C1 atom for rimantadine (see Figure 4.1), and the other lies parallel to the channel and points from the N- to the C-terminal of the M2 protein. The second vector is parallel to the line connecting between the center of the two squares formed by the C_α atoms of the 4 histidines (His37) and the 4 tryptophans (Trp41), respectively, i.e., it lies parallel to the channel and points from the N- to the C-terminal of the M2 protein. For simplicity, the second vector was termed the channel axis. The results are shown in Figure 4.6. By definition, this means that the inhibitor points its side chain along the channel in the direction to the C- or N-terminal for $\theta = 0^\circ$ or 180° , respectively.

The plots show very clearly that the two inhibitors in the 0H and 1H states were found to point their side chains in the direction toward the C terminal, and maxima of the peaks appeared at $\theta < 90^\circ$. At higher protonation states, an increase of partial charges on the His37 groups leads to a reorientation of the inhibitors. As shown in Figure 6, the transition from $\theta < 90^\circ$ to $\theta > 90^\circ$ was observed in the 2Ha-amantadine and 2Hd-rimantadine. The change of the rimantadine's orientation leads us to understand that symmetrical 2Hd diprotonation generates a stronger repulsion of the inhibitor side chain than the asymmetrical 2Ha state. In addition, an easier reorientation of amantadine (at the 2Ha state) than rimantadine (at the 2Hd state), could be due to the lower steric effect of its $-\text{NH}_3^+$ side chain in comparison with $-\text{CHCH}_3\text{NH}_3^+$ of rimantadine, especially when they were embedded in a limited space in the M2 channel.

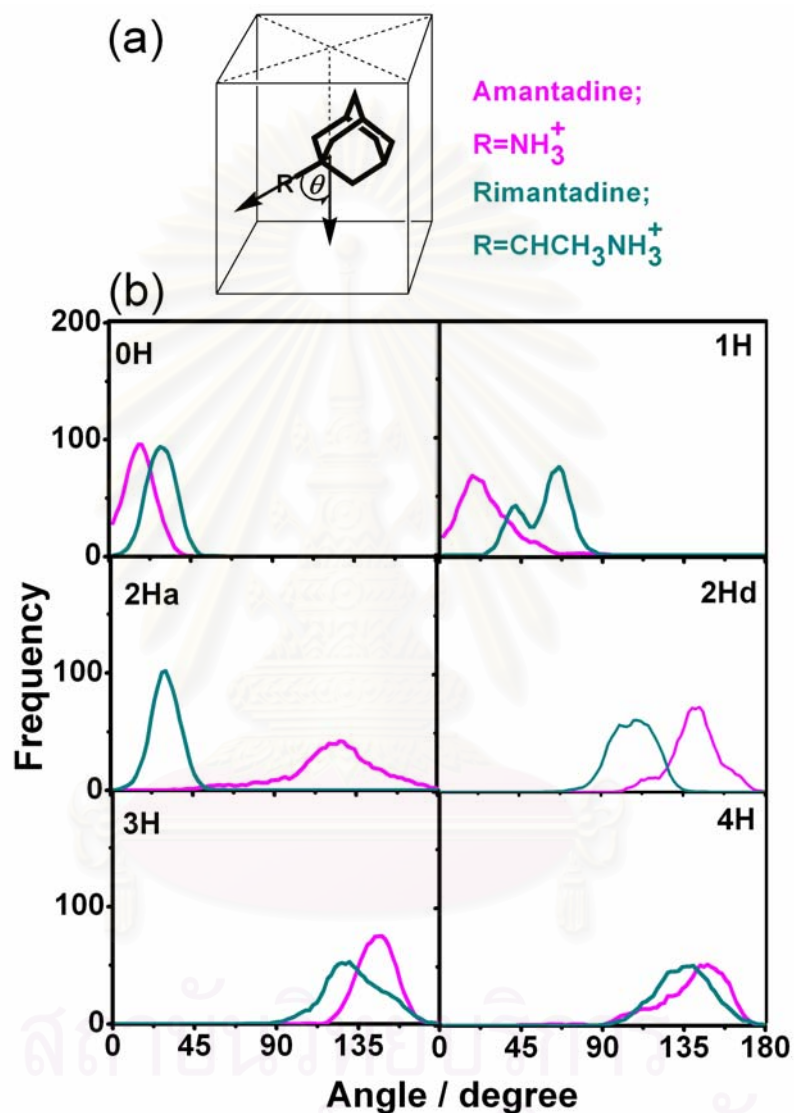


Figure 4.7 Orientation of the inhibitors. (a) Distribution of the angle θ , defined in (b) by 2 vectors, of which one points along the C-X bond (where X=N and C for amantadine and rimantadine, respectively) and the other points parallel to the M2 channel from the N- to the C-terminal (see text for details).

4.4 Conclusion

To clearly monitor the above observations in detail, the positions and orientations of the inhibitors were carefully determined from Figures 4.3, 4.4 and 4.5. They were sketched relative to the positions of the three binding residues of the M2 protein, Ala30, Ser31 and His37. The results are given in Figure 4.6. Let us consider amantadine in the 0H state as an example. It was found in Figure 4.2 to be located between Ser31 and His37 at $L \sim 16$ Å from the mouth of the pore and ~ 5 Å above the His37. Its position (Figure 4.3) is not at the center of the M2-channel, i.e., not at the center of the xy plane defined in section 3.3. It was also shown in Figure 4.4 to form hydrogen bonds with His37. In addition, its side chain was observed in Figure 4.5 to preferentially point to the N terminal with $\theta = 20^\circ$, according to the maximum of the distribution plot in Figure 4.7. With the same procedures, schematic representations of the position and orientation of the two inhibitors in the M2 channel are portrayed in Figure 4.8.

Besides a clear understanding of the preferential position and orientation of the two inhibitors for the different protonation states of the M2-protein channel, the two mechanisms of action where drugs bind to the opening pore and the His37 gate were clearly displayed (see discussion in the last part of section 4.2.4).

Taking into account all the structural data given above, the simulation results support the two previously proposed mechanisms of action of the inhibitors. The two corresponding binding sites of the inhibitors in the M2 channel are near the histidine gate (His37) and the opening pore residues (Ala30 and Ser31). In both important regions, the simulated data imply a mechanism by which the inhibitor localizes and interacts weakly with the side chains of the binding site residues and, hence, facilitates the orientation of these side chains to lie almost perpendicular to the inner surface of the channel. Efficiency of the inhibition was, then, determined by the length and bulk of the side chains of the related residues, and the order among the three residues is: His37 > Ser31 > Ala30. This hypothesis answers the question of why there is much better inhibition by rimantadine than amantadine (see Figure 4.2, and the water density in the 2Ha state). The proposed mechanisms provide a clear description toward an ultimate goal of this study, to explain how drugs inhibit water transport in the M2 protein channel.

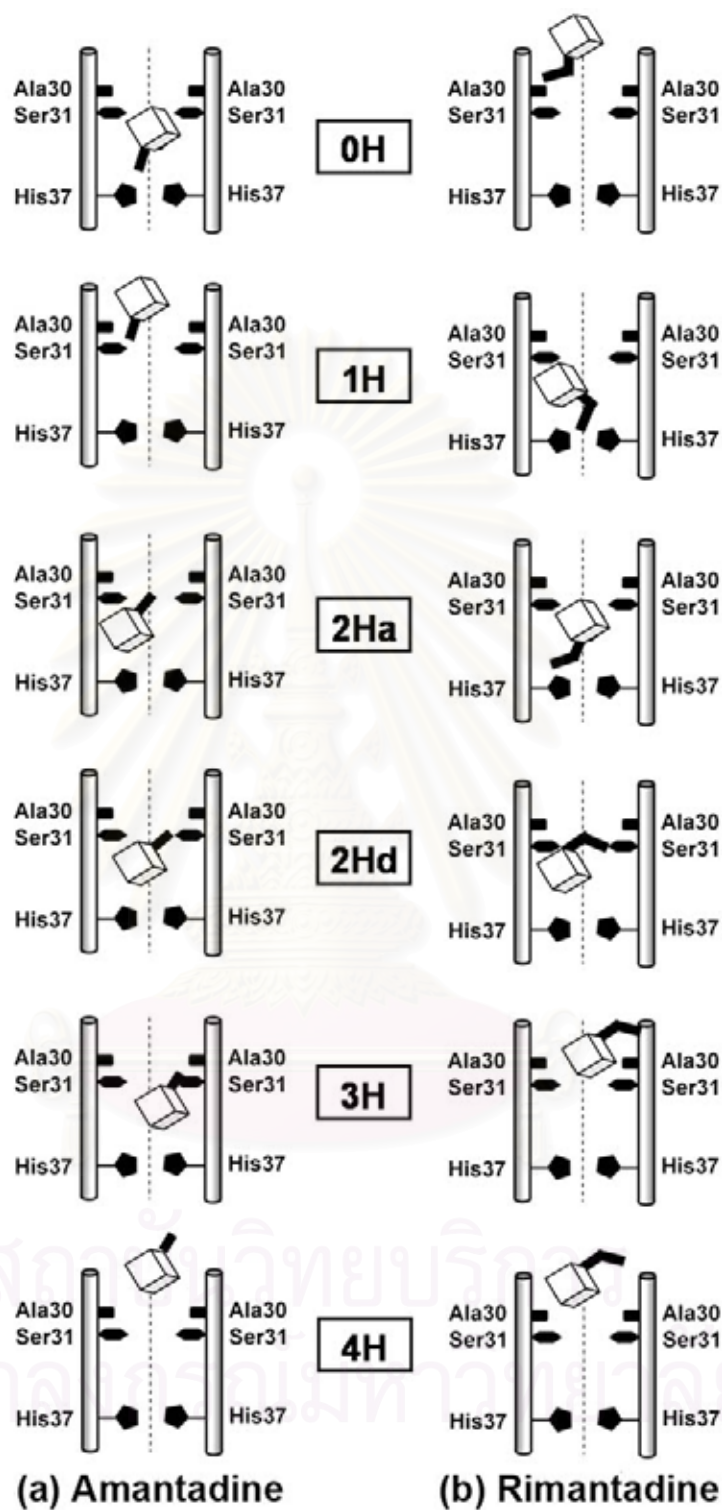


Figure 4.8 Position and orientation of inhibitors in M2 channel. Sketches showing the position and orientation of (a) amantadine and (b) rimantadine as summarized from Figures 4.3, 4.5, 4.6 and 4.7 (see text for details).

CHAPTER 5

MD SIMULATIONS OF MUTANT M2 CHANNEL-INHIBITOR COMPLEXES: A STUDY OF DRUG RESISTANCE TO AMANTADINE

5.1 Introduction

In the previous chapter, the study has addressed an important question “How drugs inhibit the M2 channel?”. The viral resistant to the amantadine drug has become a serious issue. This chapter reports the MD study of drug resistance M2 channel in order to find out “Why amantadine loses its functions in the mutant M2 proton channel?”. This is important for the prevention or prophylactics steps. To provide information to answer such question, in this chapter, a series of single M2 mutants, S31N ($IC_{50} = 267$), A30T ($IC_{50} = 3300$), and L26I ($IC_{50} = \text{unknown}$) complexed with amantadine was investigated using molecular dynamics simulations. This study aims to understand insight into drug resistant strain of influenza virus on the water transport function of M2 channel.

A recent NMR study of the M2 channel in a presence of amantadine proposed that amantadine can block either the closed or the open channel[24, 69]. Simulations were carried out for the three single mutants, S31N, A30T and L26I complexed with amantadine. To address this issue, two MD systems including non-protonation and triply-protonation states were constructed for the simulations. The results were monitored in terms of water densities, hydrogen bonding interaction between inhibitor-solvent and inhibitor-protein.

5.2 Methods

5.2.1 Construct initial model of M2 mutants and their complexes

Structure of the mutant M2 channel was built based on the model of the wild-type M2 complexed with amantadine [Protein Data Bank with the entry code: 2H95[69]. Residues in each M2 helix were mutated at positions 26, 30 and 31 using Discovery Studio 1.7 software[76, 90]. Three mutant M2 models were L26I, A30T, and S31N. Amantadine was then docked into the inner cavity of the M2 channel using

Autodock 3.0 program[84]. The resulting model for docking simulations was subsequently adjusted by manual modeling to give the final M2-drug complex.

5.2.2 Molecular dynamics simulations

Each MT-M2 complex was built according to the assigned protonation state of the M2 tetramer as described above and then was inserted into pre-equilibrated lipid bilayer, initially made up of 80 molecules of 1-palmitoyl-2-oleoyl-sn-glycerol-3-phosphatidylcholine (POPC) lipid embedded in 2445 molecules of TIP3P water[77, 78]. The simulated systems were neutralized by the counter ions and the solvated box dimensions were set to 60 x 60 x 70 Å³.

The simulations were carried out using GROMACS 3.2.1 package[71] with GROMACS force field and the Dundee PRODRG2[91] was used to generate the inhibitor's topology file. The whole structure was minimized with steepest descent algorithm. Consequently, the system was equilibrated for 0.5 ns with position restraints on the protein atoms to improve the packing of lipids around the protein, following by 8 ns MD simulations. The structural coordinate from simulations was collected every 0.5 ps for analysis.

For all simulations, the periodic boundary condition with the NPT ensemble was employed. The LINCS algorithm[74] was applied to constrain bond lengths and angles involving hydrogen atoms, and 2 fs time step was used. Systems were coupled separately to a Berendsen temperature bath at 310 K, using coupling constant τ_T 0.1 ps[80]. The constant pressure of 1 bar was kept constant by semi-isotropic coupling of the system to a Berendsen pressure bath[80]. Long-range interactions were involved within a twin-range cutoff: 1.2 nm for van der Waals interactions, and 1.2 nm for electrostatic interactions computed using the Particle Mesh Ewald (PME) algorithm[92]. The analysis phase started from 4 ns to 8 ns in which the convergences of energies, temperature, pressure, and global root mean square displacement (RMSD) were used to verify the equilibrium of the systems.

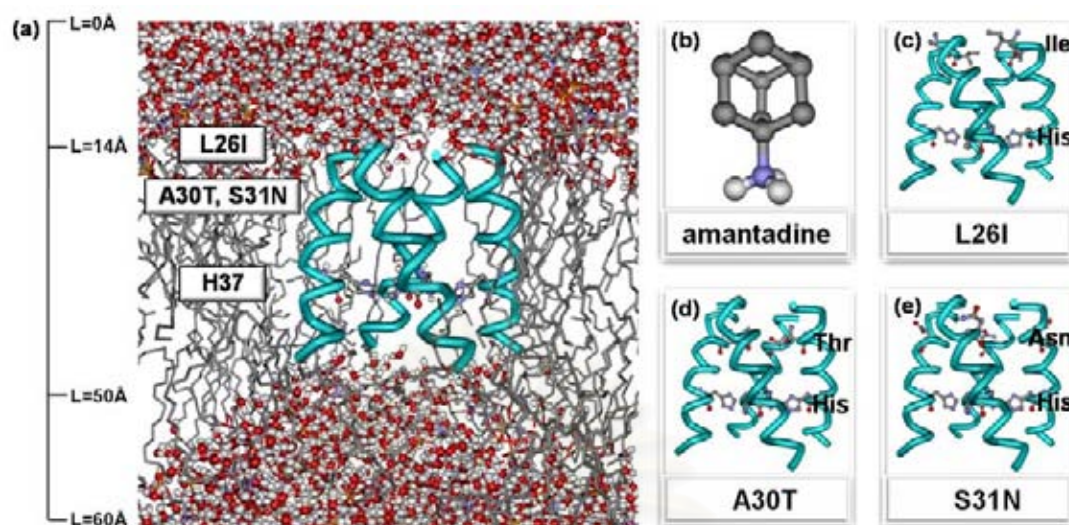


Figure 5.1 (a) The system box where the distance scale L was used for the density plot shown in Figure 5.1, $L = 14 \text{ \AA}$ and $L = 50 \text{ \AA}$ denote coordinates of the ends of the N- and C-terminal and the amantadine was zoomed into stick and ball. (b) Three single M2 mutants, L26I, A30T, and S31N.

5.3 Results and Discussion

5.3.1 Effects of the single mutant of M2 protein on its functional machinery

To determine the effects of the different single mutations on M2 protein at amino acid: 26, 30 or 31 generated resistance to amantadine, water transport was monitored in terms of water density across the mutant M2 channel as shown in Figure 5.1 where $L = 14 \text{ \AA}$ starts from the N-terminal (see Figure 5.1). Understanding the movement of amantadine and its location, relative to the histidine gate, His37, and pore lining residue, Ala30, distributions of amantadine as well as the average positions of the four histidines and four alanines were also plotted in Figure 5.2.

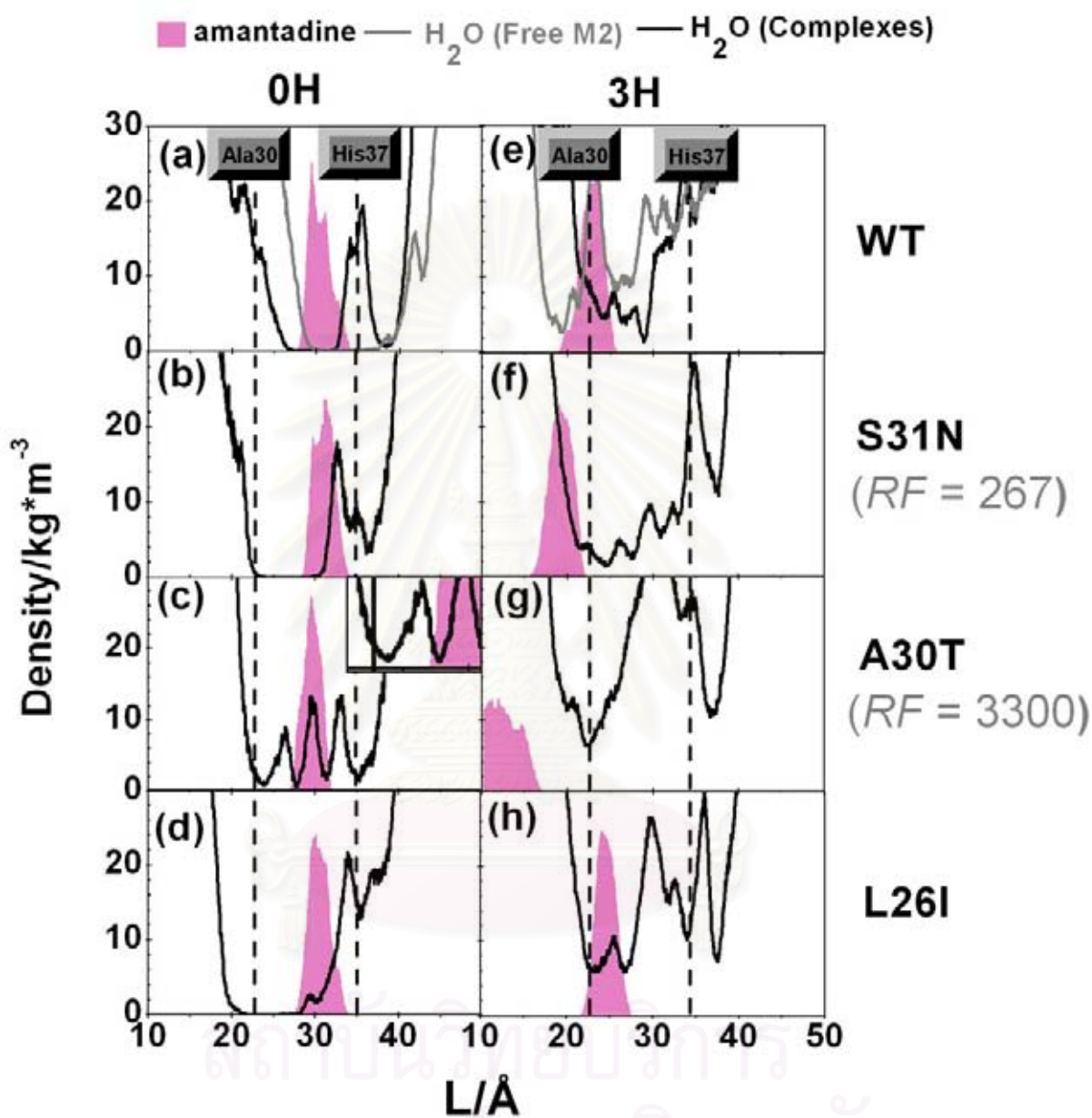


Figure 5.2 Water density along the three single mutant M2 channels (see Figure 1 for the definition of the distance L). Two protonation states (0H and 3H) of MT-M2s (S31N, A30T, L26I) complexed with amantadine are shown where the filled magenta area represents the distribution of the amantadine along the channel and the vertical dashed lines indicate Ala30 and His37. The first row shows the results of WT complexed with drug (black line) and Free M2 (gray line) (RF represents the resistant fold value of amantadine-resistance mutants compared to WT-M2 strain.[40])

The M2 protein was in the closed conformation and water cannot penetrate through the channel in the systems with uncharged histidines (OH state) of wild-type strain complexed with/without amantadine[55, 70]. Similarly, the solvent free region, where water does not permeate through the channel, was also found in the amantadine bound to S31N single mutant as shown in Figure 5.2. The situation is remarkable different for the amantadine-A30T mutant in which the OH state channel allows water to pass through (see Figure 5. 2). The information obtained from the ¹⁵N NMR [31]experiments and the MD-EVB techniques[70] suggested that the pore-opening conformation (3H state) of the M2 channel directly associated with the proton conductivity was found in the triple protonation of histidine tetrad[31, 37, 70]. Previously, we observed that less water in the 3H state of the amantadine-WT-M2 complex was detected in the middle of the pore in relative to that of the free M2 protein showing how amantadine blocked the continuous water wire. On the contrary, the water density was significantly increased in the opening of the A30T channel with amantadine bound (see the 3H state in Figure 5.2). This indicates that water freely moved through the channel and amantadine lost its capacity to block the M2 protein activity when the channel is mutated at position 30 from alanine to threonine. This observation was not seen in the amantadine bound to the S31N mutant strain: there was small amount of water at the center of the channel comparable to that of the amantadine blocked-WT-M2 protein. The simulated results were supported by the experimental IC_{50} values for the single influenza A virus recombinant M2 mutants in which the A30T mutant exhibited extremely high-level resistance to amantadine (3300-fold higher than that for wild-type strain), noticeably increased the M2 protein activity[55]. However, the function of the medium-level amantadine resistant mutant, S31N, still remained unclear due to the water densities observed in both closed and open states not shown a significant difference from those of the amantadine blocked-WT complex.

Recently, sequence analysis of the M2 gene showed that the influenza A (H5N1) viruses from Vietnam, Malaysia, Cambodia and Thailand contained double mutations (L26I/S31N) associated with resistance to amantadine[5, 6, 9], however, the IC_{50} values for this double recombinant has not been reported yet. Importance of growing problem on drug resistance to the double L26I/S31N mutant leads to the need of understanding and determining the basic function of each corresponding

single mutation, therefore another mutant (L26I) was further modeled and investigated by using MD simulations in this present study. The results are shown in Figure 5.2. The water transport along the channel cannot be taken place in the OH states of either the S31N (as explained above) or L26I single mutants (see Figure 5.2) whereas water is feasible throughout the pore in triple protonation state only in the L26I mutant strain. The data suggested that the single modeled L26I mutant could exhibit higher-level resistance to amantadine than that of the known S31N mutant.

In addition to the water density results, how influenza virus becomes resistance toward amantadine, the mobility of amantadine in the M2 channel in terms of the amantadine distribution was also measured relative to the average positions of four histidines and four alanines, where their positions face on the pore of the channel, given in Figure 5.1. Besides, the percentage and number of hydrogen bonds (hbonds) between amantadine's ammonium group and M2 protein were determined separately for the 4 units of the M2 tetramer based on the default of the GROMACS program, *i.e.*, proton donor-acceptor distance $\leq 3.5 \text{ \AA}$ and donor-H-acceptor bond angle $\geq 120^\circ$. The results are shown in Figure 5.3.

The proposed inhibitory mechanisms of antiviral drugs sensitive against the M2 ion channel were thought to be involved with the binding of inhibitor to the M2 protein at two different important sites, the opening pore residues[41, 70] and the histidine gate[31, 70]. We previously observed that inhibitor could have a higher efficiency in blocking the M2 protein machinery when it locates deeper into the center of pore of the channel and binds with His37. In complexes of amantadine bound to three different mutant strains (L26I, A30T and S31N) at the OH state, all amantadine distributions showed that amantadines are located likely in the same position and approached considerably closer to the histidine gate (Figure 5.1), consequently therefore, the hydrogen bonding between its ammonium group and the imidazole ring of His37 can be possibly formed. Number and percentage of hbonds with His37 (see Figure 5.3) in two single L26I and A30T mutants (two hbonds with 12% and 12% in OH-L26I; and a hbond with 12% in OH-A30T) were significantly lower than those of wild-type strain (two Hbonds with 56% and 17%) whereas no different importance was found in the S31N mutation in which a hbond with His37 was highly conserved (75%).

In triple protonated histidine residues of all MT-M2 complexes, amantadine was shifted toward the opening pore region (see their distributions in Figure 5.1)

especially the A30T mutation where its amantadine positioned above the channel. This result agreed with what was previously found in drug-WT-M2 complexes: inhibitor was located at shallow region of the channel in higher protonation states and subsequently formed a new interaction to the opening pore residues, Ala30 and Ser31. For the mutant systems, a hbond with Val27 (35% occupation) was made in the amantadine-S31N mutant while the drug-target interaction totally disappeared in the 3H state of the two single L26I and A30T strains (Figure 5.3). Without particular interactions with M2 binding residues, water is easily transport throughout the channel as previously mentioned.

Taken together, therefore, the ordering of detected hbond occupations in the three mutations is S31N >> L26I > A30T. This leads to the clear conclusion that resistance toward amantadine is most likely caused by a decrease in the binding of amantadine to the M2 residues as noticeably revealed in two single L26I and A30T mutant.



สถาบันวิทยบริการ
จุฬาลงกรณ์มหาวิทยาลัย

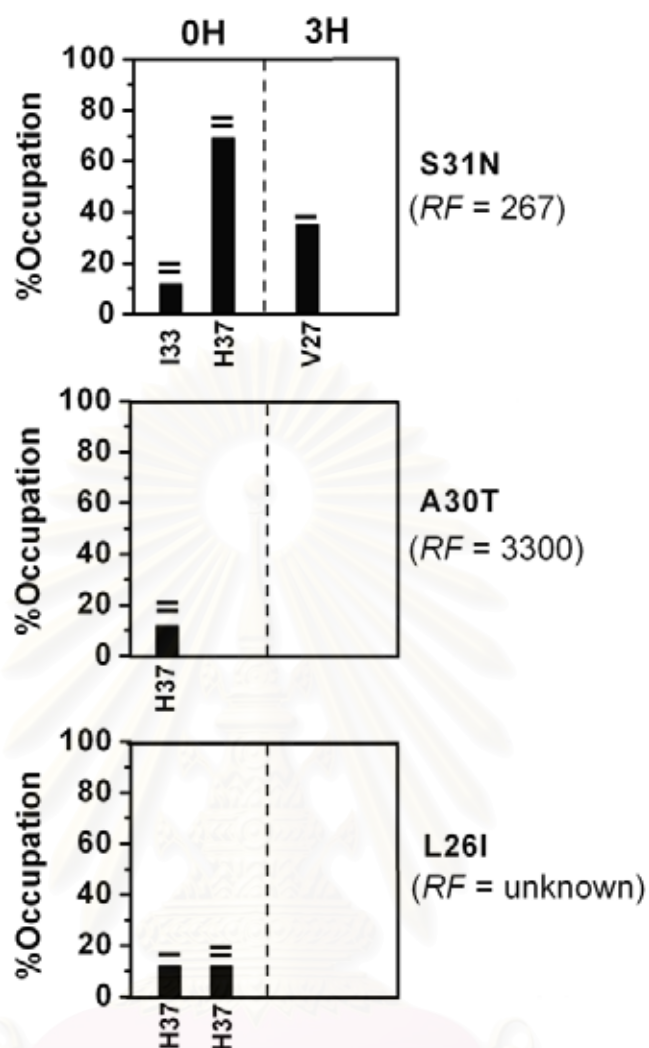


Figure 5.3 Hydrogen bond occupations between three MT-M2 residues and amantadine. The hydrogen bond occupation between residues of MT-M2 and drug for six simulated systems, where I-IV denote the four subunit of MT-M2 protein tetrad.

In summary, the obtained results provide a good correlation between the water amounts detected at the center of the channel together with the capacity of amantadine binding to His37, and amantadine-resistant level in order of A30T > S31N. Furthermore, the simulated data could help to predict the level of amantadine resistance to the single L26I mutant in which it could be higher-level resistance to amantadine than that of the S31N mutant strain.

5.3.2 Solvation of Amantadine (H-Bond with Water)

To further explore the binding between amantadine and water molecules in 0H, and 3H states, their hydrogen bonds were analyzed based on the donor-acceptor distance criteria (proton donor-acceptor distance $\leq 3.5 \text{ \AA}$ and donor-H-acceptor bond angle $\geq 120^\circ$). Percent hydrogen bonds between amantadine and water molecules of the three MT-M2 in 0H and 3H were shown in Table 5.1 compared with WT-M2. Percents of H-bonds of all three MT-M2s are dominantly high in 2-Hb and 3-Hb, while it is less preferable lower numbers of H-bonds (1-20% of 1-Hb and 2H-b). This means amantadine in all drug-MT-M2 complexes was mostly solvated by the nearest waters via the formation of two and three hbonds. In the opposition, the percent of H-bonds of WT-M2 is more preferable in 0-Hb and 1-Hb or more preferable than lower numbers of H-bond in both states (0H: 1-Hb = 60%, 3H: 1-Hb = 42%) i.e. the drug is better solvated in MT-M2. The result of drug solvation agrees very well with the % occupation between protein and drug (see Figure 5.3), namely, the more water salvation is the less % occupation between protein and drug. This shows that the major interaction is coming from the interaction between drug and water or protein.

In our simulations, the good relationship between results led us to conclude that the more accessible water in MT-M2 participating in shielding the interaction between protein and drug. Subsequently, the MT-M2s can block the less of water.

Table 5.1 The percent of H-bond (0, 1, 2, and 3) between drug and water for 0H and 3H states of three M2 mutants.

<i>M2</i>	<i>% H-bond</i>			
	0-Hb	1-Hb	2-Hb	3-Hb
0H state				
WT	23	60	16	18
S31N	1	18	77	4
A30T	2	18	47	33
L26I	1	10	39	50
3H state				
WT	25	42	26	7
S31N	1	13	52	34
A30T	1	15	38	46
L26I	1	13	59	27

5.4 Conclusions

From our simulated results, A30T mutant exhibited high-level resistance to amantadine (3300-fold higher than that for wild-type strain), noticeably increased the M2 protein activity. While S31N still remained unclear, due to the water densities observed in both closed and open states not shown a significant difference from those of the amantadine blocked-WT complex. However, the water transport along the channel cannot be taken place in the OH states of neither the S31N or L26I single mutants and it is feasible throughout the pore in triple protonation state only in the L26I mutant strain. The data suggested that the single modeled L26I mutant could exhibit higher-level resistance to amantadine than that of the known S31N mutant.

Moreover, the result of drug solvation agrees very well with the % occupation between protein and drug, namely, the more water solvation is the less % occupation between protein and drug. This shows that the major interaction is coming from the interaction between drug and water or protein. In our simulations, a good relationship between results led us to conclude that the more accessible water in MT-M2 participating in shielding the interaction between protein and drug. Subsequently, the MT-M2s can block the less of water.

CHAPTER 6

CONCLUSIONS

The structural and dynamical properties of the proton-selective M2 channel from influenza A virus were explored using molecular dynamics simulations to gain insight into proton transport across membrane bilayer. Because the transport function of M2 channel is important for viral replication process, thus the study has also investigated binding of two channel blockers, amantadine and rimantadine, which are clinically used as anti-flu agent. In addition, the thesis has also reported results from molecular dynamics study of drug resistance M2 mutant. A summary of this research project are as follows.

6.1 MD simulations of drug-free M2 channel

MD simulations of the wild-type M2 channel in the absence of the drug were carried out in a fully solvated phospholipid bilayer. Six potential protonated models were studied in order to investigate structural and dynamical basis underlying proton transport mechanism. The results show that in non-protonation (0H) state, no water across membrane bilayer was observed. This suggest that the channel is closed when the four histidine are neutral. The simulations of non-, di- (at the adjacent and opposition positions), tri- and tetra-protonation states reveal water transport through the channel, suggesting the open channel. This indicates that the channel is activated by attaching proton to N^e of His37. It is likely that the channel becomes fully opened when the four histidine are protonated.

6.2 Simulations of wild-type M2 complexed with amantadine or rimantadine

MD simulations of the wild-type M2 channel in the presence of anti-flu drugs were carried out in a fully solvated phospholipid bilayer. A simulation procedure of this study was the same protocol used in the simulations of drug-free channel. Drug binding to M2 channel was studied by simulations of different protonated models in the presence of amantadine or rimantadine. The results show the two preferential binding sites, *i.e.*, the region of pore (Leu26, Ala30 and Ser31) and the key histidine

residues (His37). Moreover, the frequency of hydrogen bonding between M2 and drugs in the simulations has been used to describe why rimantadine is a better channel blocker.

6.3 Simulations of MT-M2 complexes with amantadine

MD simulations of the mutant M2 channel (MT-M2) in the presence of amantadine were carried out in a fully solvated phospholipid bilayer. A simulation procedure of this session was the same protocol used in the simulations of two previous systems. Drug binding to MT-M2 channel was studied by simulations of two different protonated models in the presence of amantadine in which nonprotonation and triple-protonation on the histidine residues represent the closed state and open state of the channel, respectively. The simulation results agree well with the experimental result. The density of water passing throughout the high resistant A30T mutant is dominantly increased in the more protonation state, indicating the channel loses its function in the presence of amantadine. From the available data, we predicted the unknown mutation which is resistant to amantadine drug. Water molecule takes an important part to move and to cease the M2 functions.

6.4 Suggestion for further work

From this study, the important information on M2 function and drug binding were elucidated on the basis of the structural and dynamical data obtained from molecular dynamics techniques. These results would benefit for designing more potent inhibitors or improving from today drugs. However, a full series of different protonation states on the histidine residues of M2 mutants should be carried out by molecular dynamics study. Besides single mutations, double and multiple mutations are also important. This study would help to predict drug resistance to prevent the unexpected devastation from Influenza virus. In addition, QM/MM MD would also provide more and precise information, especially in the area around His37 where protonation take place.

References

- [1] World-Health-Organization. 2004. Avian influenza A (H5N1). Weekly Epidemiol. Rev. 79: 65-70.
- [2] Li, K. S., Guan, Y., Wang, J., Smith, G. J. D., Xu, K. M., Duan, L., Rahardjo, A. P., Puthavathana, P., Buranathai, C., Nguyen, T. D., Estoepangestie, A. T. S., Chaisingh, A., Auewarakul, P., Long, H. T., Hanh, N. T. H., Webby, R. J., Poon, L. L. M., Chen, H., Shortridge, K. F., Yuen, K. Y., Webster, R. G. and Peiris, J. S. M. 2004. Genesis of a highly pathogenic and potentially pandemic H5N1 influenza virus in eastern Asia. Nature 430: 209-213.
- [3] Reid, A. H. and Taubenberger, J. K. 2003. The origin of the 1918 pandemic influenza virus: a continuing enigma. J. Gen. Virol. 84: 2285-2292.
- [4] Webster, R. and Govorkova, E. 2006. H5N1 Influenza - Continuing Evolution and Spread. N. Engl. J. Med. 355: 2174-2177.
- [5] Hurt, A. C., Selleck, P., Komadina, N., Shaw, R., Brown, L. and Barr, I. G. 2007. Susceptibility of highly pathogenic A(H5N1) avian influenza viruses to the neuraminidase inhibitors and adamantanes. Antiviral Research 73: 228-231.
- [6] Barr, I. G., Hurt, A. C., Iannello, P., Tomasov, C., Deeda, N. and Komadina, N. 2007. Increased adamantane resistance in influenza A(H3) viruses in Australia and neighbouring countries in 2005. Antiviral Research 73: 112-117.
- [7] Chutinimitkul, S., Songserm, T., Amonsin, A., Payungporn, S., Suwannakarn, K., Damrongwatanapokin, S., Chaisingh, A., Nuansrichay, B., Chieochansin, T., Theamboonlers, A. and Poovorawan, Y. 2007. New Strain of Influenza A Virus (H5N1), Thailand. Emerging Infectious Diseases 13: 506-507.
- [8] Available From : http://www.who.int/csr/disease/avian_influenza/country/en/.
- [9] Cheung, C.-L., Rayner, J. M., Smith, G. J. D., Wang, P., Naipospos, T. S. P., Zhang, J., Yuen, K.-Y., Webster, R. G., Peiris, J. S. M., Guan, Y. and Chen, H. 2006. Distribution of Amantadine-Resistant H5N1 Avian Influenza Variants in Asia. BRIEF REPORT 193: 1626.
- [10] Tsiodras, s., Mooney, J. D. and Hatzakis, A. 2007. Role of combination antiviral therapy in pandemic influenza. BMJ 334: 293-294.

- [11] Ilyushina, N. A., Govorkova, E. A. and Webster, R. G. 2005. Detection of amantadine-resistant variants among avian influenza viruses isolated in North America and Asia. Virology 341: 102 -106.
- [12] Scholtissek, C., Quack, G., Klenk, H. D. and Webster, R. G. 1998. How to overcome resistance of influenza A viruses against adamantane derivatives. Antiviral Research 37: 83-95.
- [13] Bright, R. A., Medina, M.-j., Xu, X., Perez-Oronoz, G., Wallis, T. R., Davis, X. M., Povinelli, L., Cox, N. J. and Klimov, A. I. 2005. Incidence of adamantane resistance among influenza A (H3N2) viruses isolated worldwide from 1994 to 2005: a cause for concern. Lancet 366: 1175-1181.
- [14] Baz, M., Abed, Y., McDonald, J. and Boivin, G. 2006. Characterization of Multidrug-Resistant Influenza A/H3N2 Viruses Shed during 1 Year by an Immunocompromised Child. Clinical Infectious Diseases 43: 1555-1561.
- [15] Available From : <http://en.wikipedia.org/wiki/Influenza>.
- [16] Available From : http://www.who.int/csr/disease/avian_influenza/en/.
- [17] Available From :
http://en.wikipedia.org/wiki/Image:Influenza_nomenclature.svg.
- [18] Available From :
http://www.who.int/csr/disease/avian_influenza/country/cases_table_2008_04_15/en/index.html.
- [19] Available From : http://en.wikipedia.org/wiki/Image:Virus_Replication.svg.
- [20] Pinto, L. H. and Lamb, R. A. 2007. Controlling influenza virus replication by inhibiting its proton channel. Mol. BioSyst. 3: 18-23.
- [21] Pinto, L. H. and Lamb, R. A. 2006. The M2 Proton Channels of Influenza A and B Viruses. J. Biol. Chem. 281: 8997-9000.
- [22] Forrest, L. R., DeGrado, W. F., Dieckmann, G. R. and Sansom, M. S. P. 1998. Two models of the influenza A M2 channel domain: verification by comparison. Folding & Design 443-448: 3.
- [23] Forrest, L. R., Tieleman, D. P. and Sansom, M. S. P. 1999. Defining the Transmembrane Helix of M2 Protein from Influenza A by Molecular Dynamics Simulations in a Lipid Bilayer. Biophysical Journal 76: 1886–1896.
- [24] Nishimura, K., Kim, S., Zhang, L. and Cross, T. A. 2002. The closed state of a H⁺ channel helical bundle combining precise orientational and distance restraints from solid state NMR. Biochemistry 41: 13170-13177.

- [25] Takeuchi, H., Okada, A. and Miura, T. 2003. Roles of the histidine and tryptophan side chains in the M2 proton channel from influenza A virus. FEBS Letters 552: 35-38.
- [26] Chizhnikov, I. V., Geraghty, F. M., Ogden, D. C., Hayhurst, A., Antoniou, M. and Hay, A. J. 1996. Selective proton permeability and pH regulation of the influenza virus M2 channel expressed in mouse erythroleukaemia cells. J. Physiol. 494: 329-336.
- [27] Mould, J. A., Drury, J. E., Frings, S. M., Kaupp, U. B., Pekosz, A., Lamb, R. A. and Pinto, L. H. 2000. Permeation and activation of the M2 ion channel of influenza A virus. J. Biol. Chem. 275: 31038-31050.
- [28] Lear, J. D. 2003. Proton conduction through the M2 protein of the influenza A virus: a quantitative, mechanistic analysis of experimental data. FEBS Letters 552: 17-22.
- [29] Kelly, M. L., Cook, J. A., Brown-Augsburger, P., Heinz, B. A., Smith, M. C. and Pinto, L. H. 2003. Demonstrating the intrinsic ion channel activity of virally encoded proteins. FEBS Letters 552: 61-67.
- [30] Zhong, Q., Newns, D. M., Pattnaik, P., Lear, J. D. and Klein, M. L. 2000. Two possible conducting states of the influenza A virus M2 ion channel. FEBS Letters 473: 195-198.
- [31] Hu, J., Fu, R., Nishimura, K., Zhang, L., Zhou, H.-X., Busath, D. D., Vijayvergiya, V. and Cross, T. A. 2006. Histidines, heart of the hydrogen ion channel from influenza A virus: Toward an understanding of conductance and proton selectivity. PNAS 103: 6865-6870.
- [32] Wu, Y. and Voth, G. A. 2003. Computational studies of proton transport through the M2 channel. FEBS Letters 552: 23-27.
- [33] Smondyrev, A. M. and Voth, G. A. 2002. Molecular Dynamics Simulation of Proton Transport through the Influenza A Virus M2 Channel. Biophys. J. 83: 1987-1996.
- [34] Shuck, K., Lamb, R. A. and Pinto, L. H. 2000. Analysis of the Pore Structure of the Influenza A Virus M2 Ion Channel by the Substituted-Cysteine Accessibility Method. J. Virol. 74: 7755-7761.

- [35] Wang, C., Lamb, R. A. and Pinto, L. H. 1995. Activation of the M2 Ion Channel of Influenza Virus: A Role for the Transmembrane Domain Histidine Residue. Biophysical Journal 69: 1363-1371.
- [36] Venkatamaran, P., Lamb, R. A. and Pinto, L. H. 2005. Chemical Rescue of Histidine Selectivity Filter Mutants of the M2 Ion Channel of Influenza A Virus. J. Biol. Chem. 280: 21463-21472.
- [37] Hu, J., Fu, R. and Cross, T. A. 2007. The Chemical and Dynamical Influence of the Anti-Viral Drug Amantadine on the M2 Proton Channel Transmembrane Domain. Biophys. J. 93:276-283.
- [38] Intharathap, P., Laohpongspaisan, C., Rungrotmongkol, T., Loisuangsinsin, A., Malaisree, M., Decha, P., Aruksakunwong, O., Chuenpenit, K., Kaiyawet, N., Sompornpisut, P., Pianwanit, S. and Hannongbua, S. How Amantadine and Rimantadine Inhibit Water Transport in the M2 Protein Channel. (In submitted)
- [39] Ruigrok, R. W. H., Hirst, E. M. A. and Hay, A. J. 1991. The specific inhibition of influenza A virus maturation by amantadine: an electron microscopic examination. Journal of General Virology 72: 191-194.
- [40] Abed, Y., Goyette, N. and Boivin, G. 2005. Generation and Characterization of Recombinant Influenza A (H1N1) Viruses Harboring Amantadine Resistance Mutations. Antimicrobial Agents and Chemotherapy 49: 556-559.
- [41] Astrahan, P., Kass, I., Cooper, M. A. and Arkin, I. T. 2004. A Novel Method of Resistance for Influenza Against a Channel-Blocking Antiviral Drug. PROTEINS: Structure, Function, and Bioinformatics 55: 251-257.
- [42] Stouffer, A. L., Acharya, R., Salom, D., Levine, A. S., Costanzo, L. D., Soto, C. S., Tereshko, V., Nanda, V., Stayrook, S. and DeGrado, W. F. 2008. Structural basis for the function and inhibition of an influenza virus proton channel. Nature 451: 596-599.
- [43] Schnell, J. R. and Chou, J. J. 2008. Structure and mechanism of the M2 proton channel of influenza A virus. Nature 451: 591-596.
- [44] Kukol, A., Adams, P. D., Rice, L. M., Brunger, A. T. and Arkin, I. T. 1999. Experimentally based orientational refinement of membrane protein models: a structure for the influenza A M2 H⁺ channel. J. Mol. Biol. 286: 951-962.

- [45] Tian, C., Gao, P. F., Pinto, L. H., Lamb, R. A. and Cross, T. A. 2003. Initial structural and dynamic characterization of the M2 protein transmembrane and amphipathic helices in lipid bilayers. Protein Sci. 12: 2597-2605.
- [46] Wang, J., Kim, S., Kovacs, F. and Cross, T. A. 2001. Structure of the transmembrane region of the M2 protein H⁺ channel. Protein Sci. 10: 2241-2250.
- [47] Okada, A., Miura, T. and Takeuchi, H. 2001. Protonation of Histidine and Histidine-Tryptophan Interaction in the Activation of the M2 Ion Channel from Influenza A Virus. Biochemistry 40: 6053-6060.
- [48] Mesleh, M. F., Veglia, G., DeSilva, T.M., Marassi, F.M., and Opella, S.J. 2002. Dipolar waves as NMR maps of protein structure. J. Am. Chem. Soc. 124: 4206-4207.
- [49] Pinto, L. H., Dieckmann, G.R., Gandhi, C.S., Shaughnessy, M.A., Papworth, C.G., Braman, J., Lear, J.D., Lamb, R.A., and DeGrado, W.F. 1997. A functionally defined model for the M2 proton channel of influenza A virus suggests a mechanism for its ion selectivity. Proc. Natl. Acad. Sci. U.S.A. 94: 11301-11306.
- [50] Forrest, L. R., Kukol, A., Arkin, I. T., Tieleman, D. P. and Sansom, M. S. P. 2000. Exploring Models of the Influenza A M2 Channel: MD Simulations in a Phospholipid Bilayer. Biophysical Journal 78: 55-69.
- [51] Duff, K. C. and Ashley, R. H. 1992. The transmembrane domain of influenza A M2 protein forms amantadine-sensitive proton channels in planar lipid bilayers. Virology 190: 485– 489.
- [52] Wang, C., Takeuchi, K., Pinto, L. H. and Lamb, R. A. 1993. Ion channel activity of influenza A virus M2 protein: characterization of the amantadine block. J. Virol. 67: 5585-5594.
- [53] Kovacs, F. A. and Cross, T. A. 1997. Transmembrane Four-Helix Bundle of Influenza A M2 Protein Channel: Structural Implications from Helix Tilt and Orientation. Biophysical Journal 73: 2511-2517.
- [54] Sansom, M. S. P., Kerr, I. D., Smith, G. R. and Son, H. S. 1997. The influenza A virus M2 channel: a molecular modelling and simulation study. Virology 233: 163–173.
- [55] Kass, I. and Arkin, I. T. 2005. How pH Opens a H⁺ Channel: The Gating Mechanism of Influenza A M2. Structure 13: 1789-1798.

- [56] Schweighofer, K. J. and Pohorille, A. 2000. Computer Simulation of Ion Channel Gating: The M2 Channel of Influenza A Virus in a Lipid Bilayer. Biophysical Journal 78: 150-163.
- [57] Dolin, R., Reichman, R. C., Madore, H. P., Maynard, R., Linton, P. N. and Webber-Jones, J. 1982. A Controlled Trial of Amantadine and Rimantadine in the Prophylaxis of Influenza A Infection. New Engl. J. Med. 307: 580-584.
- [58] Oxford, J. S., and Galbraith, A. 1980. Antiviral activity of amantadine: a review of laboratory and clinical data. Pharmacol. Ther. 11: 181-262.
- [59] Hay, A. J. 1992. The action of adamantanamines against influenza A viruses: inhibition of the M2 ion channel protein. Sem. Virol. 3: 21-30.
- [60] Lamb, R. A., Holsinger, L.J., and Pinto, L.H. 1994. in Receptor-mediated Virus Entry into Cells. Wimmer, E., ed., pp.: 303-321.
- [61] Pinto, L. H., Holsinger, L. J. and Lamb, R. A. 1992. Influenza virus M2 protein has ion channel activity. Cell 69: 517-528.
- [62] Sugrue, R. J. and Hay, A. 1991. Structural characteristics of the M2 protein of influenza A viruses: Evidence that it forms a tetrameric channel. J. Virol. 180: 617-624.
- [63] Duff, K. C., Gilchrist, P. J., Saxena, A. M. and Bradshaw, J. P. 1994. Neutron diffraction reveals the site of amantadine blockade in the influenza A M2 ion channel. Virology 202: 287-293.
- [64] Sansom, M. S. P. and Kerr, I. D. 1993. Influenza virus M2 protein: a molecular modelling study of the ion channel. Prot. Eng. 6: 65-74.
- [65] Cady, S. D. and Hong, M. 2008. Amantadine-induced conformational and dynamical changes of the influenza M2 transmembrane proton channel. PNAS 105: 1483-1488.
- [66] Gandhi, C. S., Shuck, K., Lear, J. D., Dieckmann, G. R., DeGrado, W. F., Lamb, R. A. and Pinto, L. H. 1999. Cu (II) inhibition of the proton translocation machinery of the influenza A virus M2 protein. J. Biol. Chem. 274: 5474-5482.
- [67] Wu, Y. and Voth, G. A. 2005. A Computational Study of the Closed and Open States of the Influenza A M2 Proton Channel. Biophysical Journal 89: 2402-2411.
- [68] Kolocouris, A., Hansen, R.K., and Broadhurst, R.W. 2004. Interaction between an Amantadine Analogue and the Transmembrane Portion of the

- Influenza A M2 Protein in Liposomes Probed by ^1H NMR Spectroscopy of the Ligand. J. Med. Chem. 47: 4975-4978.
- [69] Hu, J., Asbury, T., Achuthan, S., Li, C., Bertram, R., Quine, J. R., Fu, R. and Cross, T. A. 2007. Backbone Structure of the Amantadine-Blocked Trans-Membrane Domain M2 Proton Channel from Influenza A Virus. Biophys. J. 92: 4335-4343.
- [70] Chen, H., Wu, Y. and Voth, G. A. 2007. Proton Transport Behavior Through the Influenza A M2 Channel: Insights from Molecular Simulation. Biophys. J. 93:3470-3479.
- [71] Lindahl, E., Hess, B. and Spoel, D. v. d. 2001. GROMACS 3.0: a package for molecular simulation and trajectory analysis. J. Mol. Mod. 7: 306-317.
- [72] Spoel, D. v. d., Lindahl, E., Hess, B., Buuren, A. R. v., Apol, E., Meulenhoff, P. J., Tieleman, D. P., Sijbers, A. L. T. M., Feenstra, K. A., Drunen, R. v. and Berendsen, H. J. C. (2004) Gromacs User Manual version 3.2
- [73] Leach, A. R. (1996) Molecular Modeling: Principles and Applications. Longman.
- [74] Hess, B., Bekker, H., Berendsen, H. J. C. and Fraaije, J. G. E. M. 1997. LINCS: a linear constraint solver for molecular simulations. J. Comp. Chem. 18: 1463-1472.
- [75] Cramer, C. J. (2002) Essentials of Computational Chemistry: Theories and Models. John Wiley & Sons, Ltd.
- [76] Marti-Renom, M. A., Madhusudhan, M. S. and Sali, A. 2004. Alignment of protein sequences by their profiles. Protein Science 13: 1071-1087.
- [77] Tieleman, D. P., Berendsen, H. J. C. and Sansom, M. S. P. 1999a. An alamethicin channel in a lipid bilayer: molecular dynamics simulations. Biophys. J. 76: 1757-1769.
- [78] Tieleman, D. P., Sansom, M. S. P. and Berendsen, H. J. C. 1999b. Alamethicin helices in a bilayer and in solution: molecular dynamics simulations. Biophys. J. 76: 40-49.
- [79] Jorgensen, W., Chandrasekhar, J., Madura, J., Impey, R. and Klein, M. 1983. Comparison of simple potential functions for simulating liquid water. J. Chem. Phys. 79: 926 -935.
- [80] Berendsen, H. J. C., Postma, J. P. M., Gunsteren, W. F. v. and Hermans, J. (1981) Intermolecular Forces. (Reidel, Dordrecht, the Netherlands).

- [81] Canutescu, A. A., Shelenkov, A. A. and JR., R. L. D. 2003. A graph-theory algorithm for rapid protein side-chain prediction. Protein Science 12: 2001–2014.
- [82] Humphrey, W., Dalke, A. and Schulten, K. 1996. VMD - Visual Molecular Dynamics. Journal of Molecular Graphics 14: 33-38.
- [83] Sayle, R. and Milner-White., E. J. 1995. "RasMol: Biomolecular graphics for all". Trends in Biochemical Sciences (TIBS) 20: 374.
- [84] Morris, G. M., Goodsell, D. S., Halliday, R. S., Huey, R., Hart, W. E., Belew, R. K. and Olson, A. J. 1998. Automated Docking Using a Lamarckian Genetic Algorithm and and Empirical Binding Free Energy Function. J. Comp. Chem. 19: 1639-1662.
- [85] Hermans, J., Berendsen, H. J. C. W. F. v. G. and Postma, J. P. M. 1984. A consistent empirical potential for water-protein interactions. Biopolymers 23: 1513-1518.
- [86] Berendsen, H. J. C., Postma, J. P. M., Gunsteren, W. F. v., DiNola, A. and Haak, J. R. 1984. Molecular dynamics with coupling to an external bath. J. Chem. Phys. 81: 3684-3690.
- [87] Mould, J. A., Li, H.-C., Dudlak, C. S., Lear, J. D., Pekosz, A., Lamb, R. A. and Pinto, L. H. 2000. Mechanism for Proton Conduction of the M2 Ion Channel of Influenza A Virus. J. Biol. Chem. 275: 8592-8599.
- [88] Englund, J. A. 2002. Antiviral therapy of influenza. Semin. Pediatr. Infect. Dis. 13: 120-128.
- [89] Hay, A. J., Wolstenholme, A. J., Skehel, J. J. and Smith, M. H. 1985. The molecular basis of the specific anti-influenza action of amantadine. EMBO J 4: 3021-3024.
- [90] Eswar, N., Eramian, D., Webb, B., Shen, M., Sali. A. Protein Structure Modeling With MODELLER. 2006. Current Protocols in Bioinformatics. 5.6.1-5.6.30.
- [91] Aalten, D. M. v., Bywater, R., Findlay, J. B., Hendlich, M., Hooft, R. W. and Vriend, G. 1996. PRODRG, a program for generating molecular topologies and unique molecular descriptors from coordinates of small molecules. J. Comput. Aided Mol. Des. 10: 255-262.

- [92] Darden, T., York, D. and Pedersen, L. 1993. Particle mesh Ewald: an $N\log(N)$ method for Ewald sums in large systems. J. Chem. Phys. 98: 10089-10092.



สถาบันวิทยบริการ
จุฬาลงกรณ์มหาวิทยาลัย

BIOGRAPHY

Name Chittima Laohpongspaisan

Born December 7th, 1976, Bangkok, Thailand

Education

- 1979-1983 Preprimary School
Sangmanee, Bangkok, Thailand
- 1984-1987 Primary Level
Mongkolkul Vithaya, Nakornrathchasi, Thailand
- 1988-1990 Secondary School
Sikhiu Sawadpadung Vithaya, Nakornrathchasi, Thailand
- 1991-1993 High School
Sikhiu Sawadpadung Vithaya, Nakornrathchasi, Thailand
- 1994-1997 Bachelor of Science (Chemistry)
Khon Kaen University, Khon Kaen, Thailand
- 2000-2002 Master of Science (Chemistry)
Chulalongkorn University, Bangkok, Thailand
- 2003-2007 Doctor of Philosophy (Chemistry)
Chulalongkorn University, Bangkok, Thailand

Experience

- 1998-1999 Lecturer position Department of Chemistry,
Faculty of Science, Khon Kaen University

Publications

- Intharathep, P., **Laohpongspaisan, C.**, Rungrotmongkol, T., Loisruangsin A., Malaisree, M., Decha, P., Aruksakunwong, O., Chuenpennit, K., Kaiyawet N., Sompornpisut, P., Pianwanit, S. and Hannongbua, S. How Amantadine and Rimantadine Inhibit Water Transport in the M2 Protein Channel, (*in submitted*).
- Laohpongspaisan, C.**, Rungrotmongkol, T., Intharathep, P., Malaisree, M., Decha, P., Aruksakunwong, O., Sompornpisut, P., and Hannongbua, S. Why Amantadine loses its functions in Influenza M2 mutants: MD Simulations, (*in submitted*).

* 5 Oral presentations in national and international conferences